ISSS Journal of Micro and Smart Systems (2022) 11:235–256
https://doi.org/10.1007/s41683-022-00094-9

ORIGINAL ARTICLE

Integrated photonics for RF/microwave analog signal processing of wireless systems: a review article

Fekadu Mihret[1] · T. Srinivas[1] · Gopalkrishna Hegde[1] · Preetam Kumar[1]

Received: 16 November 2021 / Revised: 16 November 2021 / Accepted: 22 January 2022 / Published online: 21 February 2022

Abstract

The continuing extensive researches and developments in integrated photonics technology have accelerated the pace of applied research in integrated microwave photonics for RF/microwave wireless systems. Integrated photonic systems outweigh their integrated electronic counterparts because of exceptional and inherent capabilities such as low loss, ultra-broadband bandwidth, high degree of reconfigurability and flexibility, immune to electromagnetic interference, and ultra-compact footprint. On the other hand, the matured semiconductor manufacturing processes have enabled the rapid advancement of optical light sources, photodetectors, modulators, and optical passive signal processors in hybrid or heterogenous integration material platforms. Thus, the successful progress in optoelectronics integration and light manipulation has underpinned the development of programmable and multifunctional photonic processors for RF/microwave analog signal processing in wireless systems. In this paper, we review the state-of-the-art advancements in integrated microwave photonic devices and systems such as microwave photonic filtering, phased array antenna photonic beamforming, and microwave photonic signal generation.

Keywords Integrated photonics · Microwave photonic filters · Phased array antenna · Optical beamforming · Microwave photonic signal generation

Introduction

Integrated photonics for RF/microwave analog signal processing is widely termed as integrated microwave photonics (IMWP). MWP deals with the generation, manipulation, transportation, and measurement of high-frequency RF signals, known as microwave signals, with the use of optical/photonic devices and technologies (Vincent et al. 2015; Preetpaul Singh Devgan 2018; Lee 2006). It has become an enabling technology in radars (Pan and Zhang 2020a), satellite communication (Abdalla et al. 2019), 5G networks (Mihret et al. 2020; Balakier et al. 2020), radio astronomy (Norris and Bland-Hawthorn 2019). The key driving factors behind on the use of optical domain processing of RF/microwave signals in wireless communication systems are the inherent broadband bandwidth of optical signals, the low loss of integrated optical waveguides and optical fibers as media of transportation, the flexibility of tailoring or manipulating the amplitude or phase responses of RF signals over large bandwidth, and the compact footprint and lightweight of optical devices as compared to traditional RF/microwave circuits. On the other hand, the early demonstrations of MWP were in bulky fiber-based devices and systems which are relatively expensive and susceptible to environmental variations such as mechanical vibrations and temperature fluctuations. Therefore, the advancement of integrated photonics technology where light sources, modulators, microwave optical processors, and photodetectors are encompassed in one or hybrid material platforms (Kuar et al. 2021), has played

✉ Fekadu Mihret
fekadug@iisc.ac.in

T. Srinivas
tsrinu@iisc.ac.in

Gopalkrishna Hegde
gopalkrishna@iisc.ac.in

Preetam Kumar
preetamkumar@iisc.ac.in

[1] Department of Electrical Communication Engineering, Applied Photonics Lab, Indian Institute of Science, Bengaluru, India

significant roles in alleviating the aforementioned challenges. Besides, integrated photonics enhances light matter interactions, confining light in small volumes. This in turn enhances the performances of optical devices like large modulation bandwidths, high spectral resolution, high degree of reconfigurability, and high signal-to-noise ratio (SNR) performance. The combined influence of full integration, advanced functionalities, and high performance have been the main attractive features of IMWP for research communities in the area (Marpaung et al. 2019).

Working principles of IMWP

The typical IMWP system consists of three major subsystems, namely, electrical to optical conversion (E/O) with a laser source, an optical modulator, and an input RF source, the optical processing with optical signal processor, and optical to electrical conversion(O/E) with photodetection as shown in Fig. 1.

The optical modulator takes the laser source with center frequency f_c and the RF signal with center frequency f_{RF} and produces three signal components: optical carrier with f_c, two optical side bands with center frequencies $f_c + f_{RF}$ and $f_c - f_{RF}$. As we see, the two optical side bands carry RF information which usually comes from RF antenna. These three signal components are fed to integrated optical processor for various RF/microwave processing functionalities such as filtering, phase shifting, beamforming, frequency up/down-conversion, frequency generation, frequency measurement, and so on. After processing of RF/microwave signals in optical domain, the optical detector converters back to RF/microwave domain for postprocessing in RF circuits and digital signal processors. The main point we should note is that the signal processing functionalities in optical domain are translated to RF domain after photodetection, for example filter responses.

Material platforms for integrated microwave photonics

Optical materials are the main ingredients of the integrated microwave photonics signal processors. Diverse range of the processors' functionalities needs different material physical properties such as refractive index, bandgap, two-photon absorption, second-order nonlinearity, nonlinear refractive index, electro-optical coefficient, thermo-optic coefficient, piezoelectric coefficient, and waveguide propagation loss (Kuar et al. 2021). Table 1 lists some of the most commonly used optical waveguide materials together with the material properties.

The refractive index is an important property of the optical waveguides as it determines the relative index contrast with the surrounding materials. The high refractive index contrast helps to confine light inside the guiding core and this in turn reduces footprint and enhances higher integration density. But, high index contrast has a disadvantage as it incurs high loss of optical power or energy.

The bandgap energy level determines the wavelength region where low absorption or low loss occurs; in photodetectors, it determines the longest wavelength where detectable or absorbed photons can generate electron–hole pairs; in nonlinear applications, it determines the shortest wavelength where two-photon absorption occurs; for semiconductor light sources and amplifiers in direct band gap materials, it determines the wavelength at which electron–hole pairs recombine and emit or amplify coherent light.

The nonlinear effects of materials play significant role in optical signal processing and frequency generation (Boyd 2008; Langrock et al. 2006). The second-order nonlinearity enables important optical processes such as second-order harmonic generation, sum frequency generation, parametric down-conversion, and difference frequency generation (Langrock et al. 2006; Chang et al. 2021). The Kerr effect in the third-order nonlinearity helps in the realization of self-phase modulation, cross-phase modulation, and four-wave mixing. Particularly, the nonlinear refractive index helps in generating optical frequency combs by using microring resonators (Del'Haye et al. 2007; Li et al. 2021).

Many optical materials exhibit thermo-optic effect which is the exchange of refractive index of the material with temperature. The thermo-optic coefficient, which is the degree of the refractive index change per degree kelvin temperature increase, characterizes the effect of temperature on the materials. Most of programmable and reconfigurable photonic devices use the thermo-optic effect to

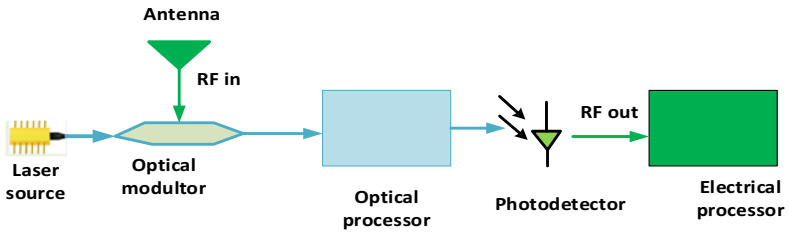

Fig. 1 Block diagram of RF to optical conversion, processing, and conversion back to RF in electrical domain

Table 1 Physical properties of various optical materials (Kuar et al. 2021)

Material property/technology parameter	Silicon (SiO2 BOX)	Si_3N_4 (SiO2 BOX)	SiO2 (doped)	GaAs (native grown)	GaAs (SiO2 BOX)	InP (native grown)
Refractive index (at 1.55um)	3.47	2.00	1.45	3.67	3.67	3.17
Refractive index contrast (at 1.55um)	2.22	0.53	0.003–0.011	0.233	2.22	0.03–0.77
Bandgap type	Indirect	Indirect	Indirect	Direct	Direct	Direct
Band gap energy (eV)	1.14 (1.09 μm)	5 (0.25 μm)	9.3 (0.13 μm)	1.43 (0.86 μm)	1.43 (0.86 μm)	1.34 (0.93 μm)
Two-photon absorptions (cw/GW)	1.5	0	–	27	27	24–33
Second-order nonlinearity (pmV^{-1})	–	–	–	119	119	–
Nonlinear refractive index (Kerr coefficient) n_2 ($m^2\ W^{-1}$)	5×10^{-18}	2.4×10^{-15}	1.15×10^{-19}	1.59×10^{-17}	1.59×10^{-17}	–
Electro-optical coefficient (pm/V)	–	–	–	$r_{41} = 1.5$	$r_{41} = 1.5$	—
Thermo-optic coefficient (K^{-1})	1.8×10^{-4}	2.4×10^{-5}	0.8×10^{-5}	2.67×10^{-4}	2.67×10^{-4}	1.94×10^{-4}
Piezoelectric coefficient (pc/N)	–	–	–	$d_{14} = 2.6$	$d_{14} = 2.6$	–
Mode Size (μm^2)	10–0.1	< 1	30–80	1–1.5	0.5	1–1.5
Waveguide propagation loss (dB/cm)	0.1–3	< 0.1		1.6	4	< 0.5

control the phase and intensity of the light (Pérez et al. 2018).

Some materials, for instance LiNbO3, lead zirconate titanate (PZT), and quartz, change their mechanical structure when an electric field is applied, and this is termed as piezoelectric effect and the material is characterized by piezoelectric coefficient. This mechanic deformation or change in physical length with an applied electric field is important in the tuning of the central frequency of operation, the phase and intensity of light in many programmable and reconfigurable photonic devices, for example in microring resonator-based devices (Jin et al. 2017).

When it comes to the full integration concept of microwave photonic devices, one can ask the question, is it possible to integrate light sources, modulators, signal processors, and photodetectors in one material platform? The answer is that it is not possible to integrate in a single material platform since some materials are weak in some performances; for example, silicon is an indirect bandgap material and hence it cannot be used for light source and photodetector implementations. To tackle these problems and utilize the advantages of full integration, intense research has been started in hybrid and heterogeneous integration. The hybrid integration is the process in which two or more photonic integrated circuits are connected from different material platforms into one single package (Kuar et al. 2021). In this process, packaging is performed after individual integrated circuits have been fabricated and tested. For example, the fully processed III–V photonic chips such as laser source chips and photodetector chips, amplifier chips, silicon, and silicon–nitride-based passive integrated processors have been integrated in one package. These chips can be mounted either directly on the top of the integrated circuits or next to them. Another powerful integration technique is heterogenous integration process in which two or more material technology platforms are combined into a single photonic integrated photonic chip. For example, thin-films of III–V materials are grown on silicon or silicon nitride platforms so that lasers, modulators, photodetectors, and passive processors can be integrated in a single large photonic chip. Detailed treatment of heterogenous integration is covered in Komljenovic et al. (2016).

Optical modulation for IMWP

Optical modulators are the most important parts of IMPW as well as in optical communication systems. The advancement of materials' technologies and fabrication methods have underpinned the sustained research in high-performance optical modulators (Burla et al. 2019; Chen et al. 2015; Weigel et al. 2018; Boynton et al. 2020; Nazoki et al. 2017; Kuo et al. 2006; Nedeljkovic et al. 2011; Dong et al. 2012, 2013; Sepehrian et al. 2019; Wu et al. 2020; Sato et al. 2017; Sinatkas et al. 2021; Lauermann et al. 2014; Lauermann et al. 2016; Zhou 2016; Zhou and Yu 2009). Optical modulators superimpose an electrical or microwave signals onto an optical carrier. The information to be encoded into optical carrier is amplitude, phase, frequency, and polarization of the information signal.

Under the influence of applied external electric field, the three most commonly employed physical effects, namely,

Pockels and Kerr electro-optic effects, Franz–Keldysh and quantum-confined Stark effect, and free-carrier effect (plasma dispersion effect) control the phase and amplitude of modulation. In the Pockels effect, the ordinary and extra ordinary refractive indices of non-centrosymmetric crystalline materials change proportional to the applied static (DC) or low frequency, compared to optical frequency, electric field. The Kerr effect is similar to Pockels effect, but the refractive index changes in proportion to the square of applied electric field. The common modulators under these effects are based on lithium niobate ($LiNbO_3$) (Burla et al. 2019; Chen et al. 2015; Weigel et al. 2018). Franz–Keldysh and quantum-confined Stark effects characterize the change in absorption spectrum band edge of a semiconductor material with applied external field. Franz–Keldysh effect occurs in bulk materials while quantum-confined Stark effect occurs in quantum wells. The modulators under these effects are called electro-absorption modulators (Nazoki et al. 2017; Kuo et al. 2006) and most of the design of these modulators have been relying on III–V semiconductor materials. In free-carrier effect (plasma dispersion effect), the absorption and refraction optical properties change when the injected free-carrier concentration changes, which is the phenomenon in semiconductors. The change in refractive index and absorption of the material aids in controlling the amplitude and phase of the light being guided. The modulators (Nedeljkovic et al. 2011; Sepehrian et al. 2019; Sato et al. 2017) based on plasma dispersion effects have usually been designed using silicon material. An extensive review on electro-optic modulators is found in Sinatkas et al. (2021).

The commonly used physical architectures or waveguiding structures for phase and amplitude modulation are simple straight waveguide-based modulators, Mach–Zehnder interferometer-based modulators (Zhou 2016), advanced modulators based on combination of Mach–Zehnder interferometers and phase modulators (Zhou and Yu 2009) and microring resonator-based modulators (Dong et al. 2013).

Integrated microwave photonic filters

Microwave Photonic filters (MWPF) are one of the most important signal processing functionalities in filtering of unwanted portion or noise from the input RF/microwave signals (Marpaung et al. 2019), and applicable in diverse areas such as satellite and wireless communication systems, radar systems, sensors, and radio astronomy. Unlike conventional electronic RF filters, MPFs possess wideband tunability, high resolution, bandwidth reconfigurability, and immunity to electromagnetic interference, compact footprint, and low loss. In most of RF/microwave signal filtering, there are stringent requirements of high spectral resolution, wideband operation, bandwidth and center frequency tunability, and stability to environmental hostilities. Therefore, it is important to research MWPF which can meet the above requirements as much as possible. In the literature world, there are two approaches of designing MWP filters: the first is based on discrete circuit components—this approach is bulky in implementation and susceptible to environmental variations, for instance fiber-based filters, and the second is based on integrated circuit platform—this approach is economically viable, compact in footprint and stable to the environmental variation.

Principles of microwave photonic filtering

There are three mechanisms for the implementation of RF/microwave optical filtering: (1) Multitap interference-based optical domain filtering. In this scheme, RF-modulated sidebands are tapped to multiple branches where each branch has amplitude scaling, time delaying, and phase shifting functions. After these manipulations, the contributions from all taps or branches are summed. The summation produces a desired optical filter response which is the resultant of all taps. Then after photodetection, the multitap optical filter response is directly transferred to RF filter response. The amplitude, time delay, and phase control in each optical tap produces the desired RF filter response. (2) Direct transfer of optical filter response to RF filter response: in this scheme, the RF-modulated optical sidebands are processed using optical filter and photo-detected or down-converted to transfer directly the optical response to RF response. (3) Hybrid approach, direct optical filter response transfer plus RF self-interference at photodetection: in this approach, the phase modulator produces two RF-modulated optical sidebands which are 180 degrees out of phase and optical filter controls the sidebands to equalize their amplitudes for complete constructive and destructive interference during photodetection. At frequencies where the phase difference is 180 degrees, complete destructive interference occurs, provided that amplitudes are properly equalized by optical filter.

Integrated two-tap microwave photonic filter based on photonic crystal was demonstrated for both notch and bandpass filters that can be tuned over 0–50 GHz center frequency range (Sancho et al. 2012). The two taps are implemented based on the polarization of modal fields, i.e., TE and TM modes. When TE and TM modes propagate through the crystal waveguide, they experience different time delays and attenuations since each mode has different group index and hence forms two taps. In Xu et al. (2019), transversal photonic RF filters, with 80 taps based on 49 GHz free spectral range integrated micro-combs using ring resonators, has been demonstrated with significantly

increased performance in terms of high-quality factor, high out-of-band rejection up to 48.9 dB, a reconfigurable 3 dB bandwidth from 0.4 GHz to 4.6 GHz, and ability to generate arbitrary filter shapes. The amplitudes of frequency combs are controlled by wave shapers which alters weighting taps and the time delay spacing between adjacent frequency comb lines is generated by dispersive fibers. Even though the reported multitap RF filter signifies high-performance achievements, the architecture is not implemented in integrated form since it uses fibers and wave shapers based on lens to control the amplitude weights and time delays.

Multiple demonstrations have been presented using direct optical filter response shape transfer to RF filter response (Fengjie et al. 2018; Liu et al. 2018; Taddei et al. 2014). In (Fengjie et al. 2018), thermally tunable microwave notch filter based on a single over-coupled microring resonator has been proposed and the performance of 56 dB rejection ratio and a quality factor of 48,500. Another a silicon-on-insulator-based widely tunable microwave photonic notch filter based on under-coupled microring resonator and two cascaded tunable Mach Zehnder interferometers (MZIs) has been experimentally demonstrated (Liu et al. 2018). The device achieves peak rejection ratio exceeding 60 dB and 3 dB bandwidth tunability of 780 MHz, and a center frequency tunability range of 0–40 GHz. Taddei et al. (2014), a high spectral resolution bandpass filter based on nine coupled resonator optical waveguides (CROWs) has been presented in TriPleX^{TM} technology and the filter is intended to the selection of a channel in a dense frequency-division subcarrier satellite communication system. By tuning the phases on feedback paths of CROWs and their power coupling coefficients, the center frequency can be tuned over entire range of FSR of 1.4 GHz and bandwidth can be tuned in tens of MHz.

In hybrid approach, direct optical filter response transfer plus RF self-interference at photodetection, many demonstrations have been reported (Marpaung et al. 2014; Liu et al. 2017a; Liu et al. 2017b; Zhuang et al. 2015; Jiang et al. 2018; Li et al. 2019). A notch filter with ultra-high rejection ratio up to 66 dB was demonstrated in Marpaung et al. (2014) using a single microring resonator and a dual-parallel Mach–Zehnder modulator (DPMZM). The filter is based on the mixing of two out of phase RF signals of the same frequency when the beating occurs between optical carrier and the two optical sidebands at the photodetector. The microring resonator is in the over-coupled mode and should maintain 180-degree phase shift and equal amplitudes between the two sidebands by tuning its coupling coefficient. When amplitude and out of phase matching happens, there is complete destructive interference at the notch filter and hence ultra-high rejection ratio regardless of the microring resonator's notch value. The downside of this notch filter is that it is not tunable in bandwidth and center frequency range. However, bandwidth and center frequency tunable high-resolution IMWP filter based on two cascaded microring resonators, operating in over-coupled and under-coupled modes, has been demonstrated in Liu et al. 2017a. The center frequency is tunable from 1 to 12 GHz range and the bandwidth is tunable from 150 to 300 MHz Over-coupled microring resonator provides a phase shift of 180 degree for upper sideband while under-coupled microring resonator provides 0 degree for lower sideband. Thus, the intensity modulated two optical sidebands having nearly identical amplitudes at notch frequency are out of phase and interfere destructively in RF domain after photodetection, the beating of the carrier frequency with the two sidebands. In (Liu et al. 2017b), the same authors, as of Liu et al. 2017a, has reported the same filter configuration but including high RF performances achievements such as high link gain of 8 dB, a low-noise figure (NF) of 15.6 dB, spurious free dynamic range (SFDR) of 116 dB · $Hz^{2/3}$ and stop band rejection of 50 dB. Besides, the same concept has been extended to operate the filter in dual frequency bands by adding two more microring resonators operating in under-coupled and over-coupled modes. We provide, as an example for filtering process, the experimental setup and the results of Liu et al. 2017b in Figs. 2, 3, and 4.

An exciting work on the programmable photonic chip for RF filter implementations and other various functionalities has been demonstrated (Zhuang et al. 2015). The photonic chip is composed of two-dimensional interconnected Mach–Zehnder interferometer meshes as shown in Fig. 5**.** In each MZI, there two-phase shifters: one in upper arm and another in the lower arm, and two-phase shifters in input–output couplers. By tuning couplers in bar or cross-state, different optical paths can be selected such as single microring structure, cascaded microrings, and coupled microrings, and the phases of the propagating light can be controlled using the phase shifters on the arms.

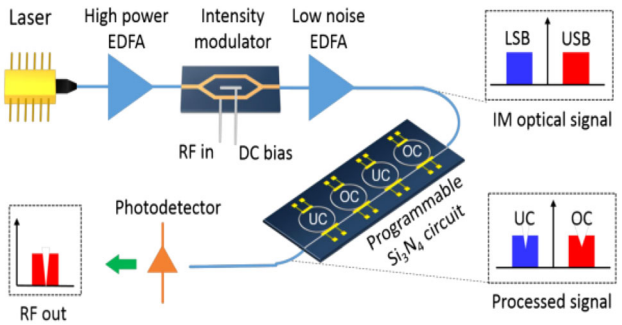

Fig. 2 Experimental setup showing conceptually the filtering processes (Liu et al. 2017b). © 2017 OSA

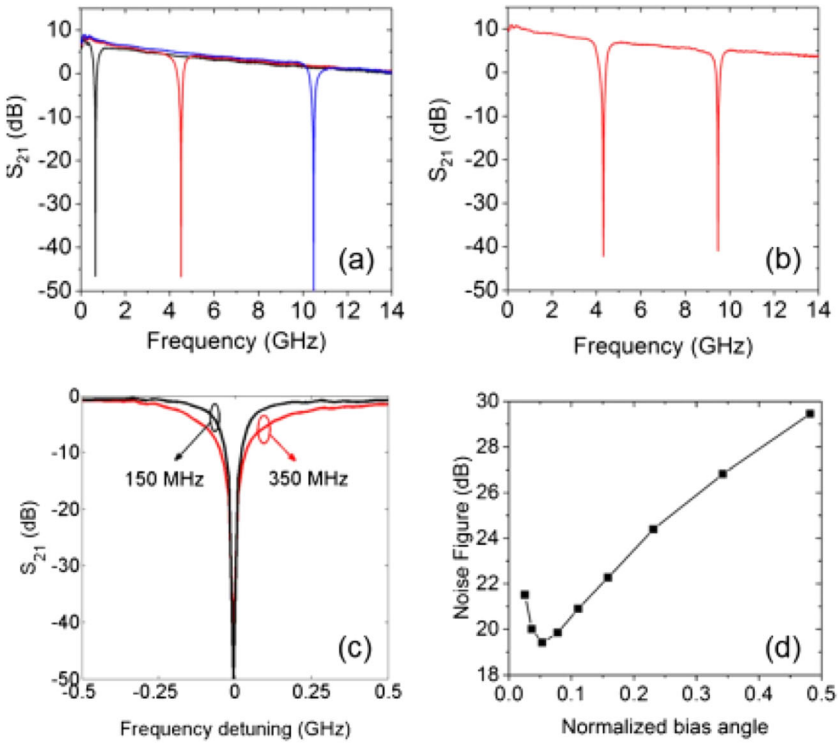

Fig. 3 Response of **a** single-band filter, **b** dual-bandpass filter, **c** bandwidth tuning, and **d** NF vs normalized bias angle at 6 GHz (Liu et al. 2017b). © 2017 OSA

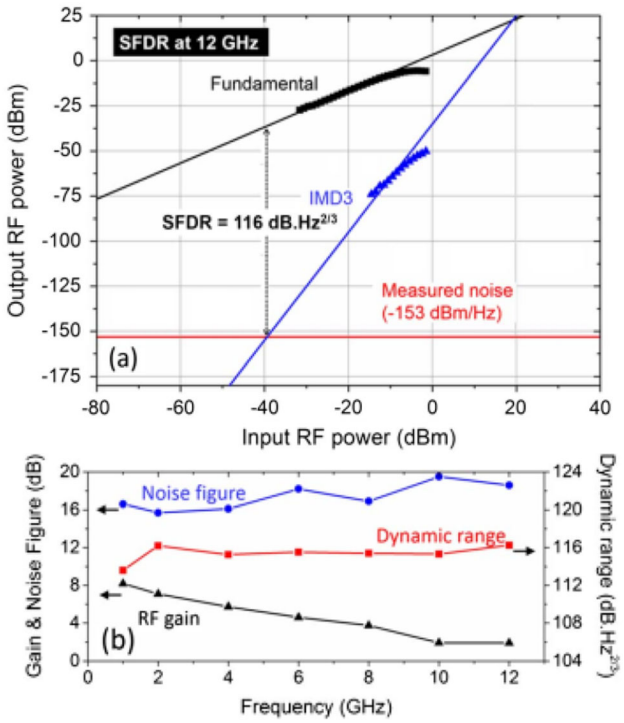

Fig. 4 Measured **a** SFDR at 12 GHz and **b** RF gain, NF and SFDR overall frequency range (Liu et al. 2017b). © 2017 OSA

Figure 5 shows schematic MxN two-dimensional waveguide mesh network with MZI as an interconnecting cell for the pathways. By programming the MZI meshes we can have various circuit topologies as shown in Fig. 5b–d. In case of RF filtering demonstration, two cascaded ring resonators are selected by programming multiple pathways as shown in Fig. 6. RF signals and continuous wave laser source are superimposed by the intensity modulator and fed to the microring resonators which are either in under-coupled or over-coupled modes. The two optical sidebands become in phase after passed through respective microrings (lower sideband matches with one microring notch frequency and upper sideband matches with another microring notch frequency). If both microrings' notch frequencies are in phase, that is, in the same coupling mode (microrings are either under-coupled or over-coupled mode), the photodetection produces constructive RF interference; both sidebands add up constructively resulting in the notch filter response as we can observe in the upper inset (iii) of Fig. 6. We have to note that destructive interference can also produce the same filter response as we have discussed in the papers of Liu et al. 2017a; b). The bandpass filter response is obtained in the same way as notch filter response with an addition that the carrier frequency is at 90-degree phase shift to invert notch response to bandpass response in the photodetection stage as shown in the lower inset (iii) of Fig. 6. Measured band-stop and bandpass filter responses of the multifunctional programmable processor are shown in Fig. 7 with center frequency tunability.

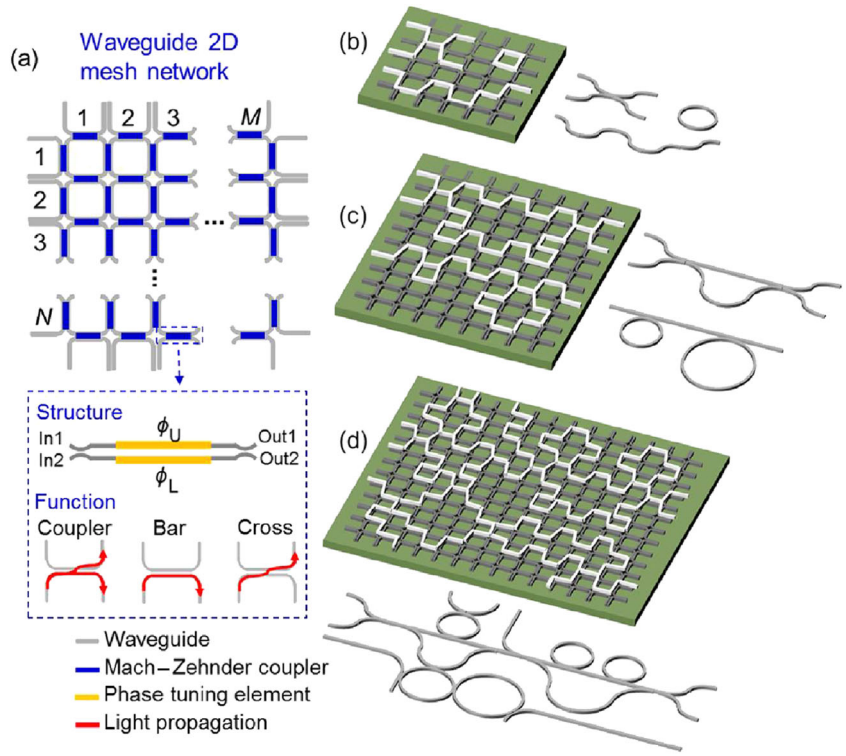

Fig. 5 **a** Grid of MxN MZI-waveguide mesh network and **b–d** few functionalities implemented by programming MZI-based mesh networks (Zhuang et al. 2015). © 2015 OPTICA

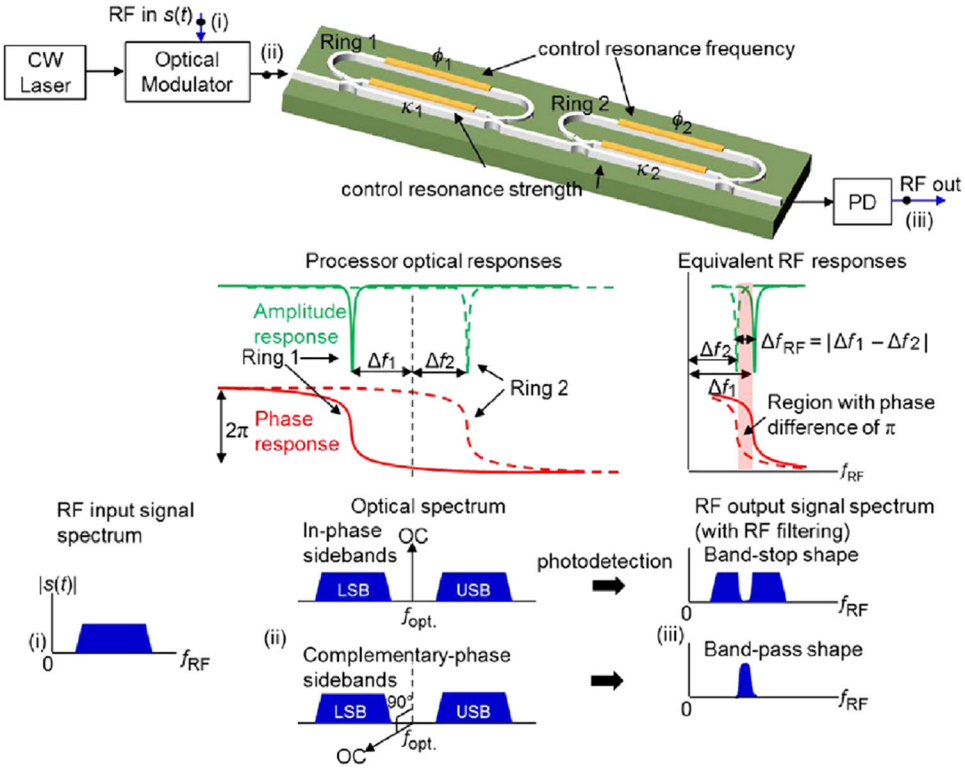

Fig. 6 Microwave photonic filtering implementation using programmable meshes. *CW* continuous wave; *LSB/USB* lower/upper sideband; *OC* optical carrier; *PD* photodetection [44]. © 2015 OPTICA

To add more, a tunable bandpass IMWP filter has been reported (Jiang et al. 2018) by using a single microring resonator operating in a notch response and optical phase modulator. The phase modulator produces two 180 degrees out of phase RF-modulated optical sidebands and the upper sideband aligns with the microring's shallow or small notch frequency response and hence suppressed at the output of the microring. The passbands of the notch

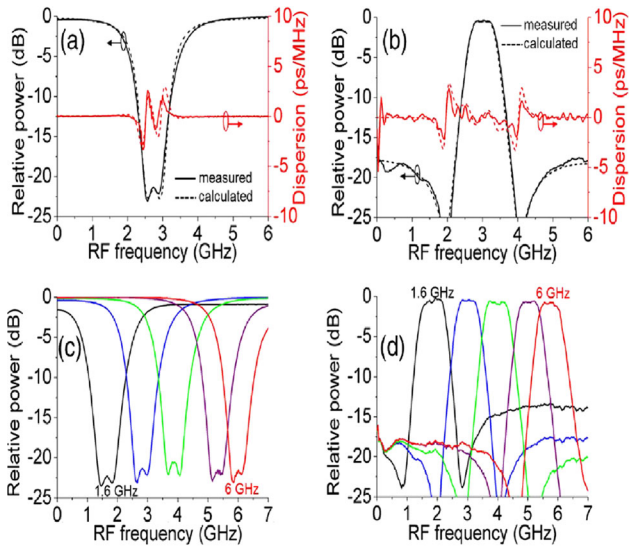

Fig. 7 **a**, **b** Measured band-stop and bandpass filter responses and theoretical curve fitting and **c**, **d** center frequency tunability (Zhuang et al. 2015). © 2015 OPTICA

response and lower sideband are out of phase with equal amplitude. Therefore, at photodetection, small partial interference occurs in the notch region and destructive interference occurs in the rest of the regions, resulting in the passband response. However, the microring's residual phase degrades and limits the filter's out-of-band rejection ratio and the shape factor. These limitations have been tackled by using dual optical carriers, with their wavelengths oppositely detuned from the two resonant frequencies of a notch microring resonator. Thus, the residual phase induced outside of the notch region of RF frequencies is reduced and the out-of-band rejection ratio and shape factor are greatly enhanced. In contrast with the single carrier method, out-of-band rejection ratio is improved from 17.7 dB to 31.5 dB, and the filter's shape factor is enhanced from 3.05 to 1.78. Moreover, by varying the wavelengths of the dual carriers and coupling coefficient of the ring resonator, the center frequency is tunable from 2 to 14 GHz range and 3 dB bandwidth is tunable from 0.673 to 2.798 GHz range. Table 2 summarizes the performance comparisons of some reports on integrated microwave photonic filters.

Integrated microwave photonic beamforming for phased array antennas

In today's RF/microwave wireless communications systems, phased array antennas are the key enabling technological achievements providing high link gain, increased capacity through spatial multiplexing, and improved signal-to-noise ratio (SNR) by boosting signal strength and mitigating interferences from other users. For example, a broadband 5G millimeter-wave beam steering/beamforming requires high gain, pencil-like directional narrow beam transmitted and received signal patterns in order to accommodate and track movable ultra-high number of users and devices utilizing internet of things (IOT) technology. These stringent requirements can only be achieved by carefully designed and implemented phased array antennas and beamforming networks which consist of phase shifters, amplitude tapers, and true-time-delay lines (TTDs). However, integrated electronic circuits controlling amplitudes and phases of beamforming networks pose significant challenges of bandwidth bottleneck and high-insertion losses at millimeter-wave frequencies. Therefore, to solve these challenges integrated photonic circuits with inherent ultra-broadband and low losses are viable solutions for broadband RF/microwave beamformers.

Working principles of RF/microwave phased array antenna beamforming

Isotropic and nondirective antennas radiate power in all directions and receive from all directions regardless of the location of the terminal user. This phenomenon wastes the transmitted power, significantly reducing the received power and degrading the SNR since the link gain is small and interference from other users is high. By spatially directing or focusing the radiated signal, the information transmission energy consumption can be efficiently optimized, and parallel data streams carried on the same frequency can be spatially demultiplexed by minimizing spatial interference. Besides, the transmitter antenna array with the same transmit power of each element, the overall received signal strength can be boosted by summing up/combining the received signal from each antenna element of the receiver antenna array.

A typical RF phased array antenna transmitter with four antenna elements is shown in Fig. 8 to illustrate the concept of beamforming/ beam steering (Cao et al. 2016). The designations d, θ, τ, are physical spacing between adjacent antenna elements, the beam steering direction, and time delay between signals fed to adjacent antenna elements, respectively. If there is no delay or phase shifter network, the signals reach at the wavefront at different time delays and phases which cause signal distortion. So, for the waves radiated from each antenna to propagate with identical phase and combine constructively, the delay or phase compensation mechanism is required, which is called beamforming network. As we can observe in Fig. 8, the wavefront, which is perpendicular to radiation direction, aligns with antenna one (Ant1) and signal radiated from this antenna has no delay. But the signal of Ant2 is delayed by τ, that of Ant3 and Ant4 are delayed by 2τ, 3τ,

Table 2 Summary of some performance reports of integrated microwave photonic filters

Architecture/ technology	Filter type	Material platform	Fixed non-tunable bandwidth (GHZ)	Bandwidth tuning range (GHz)	Center Frequency Tuning range (GHz)	Rejection ratio (dB)	Maximum Q-factor	Refs.
Ring resonator	Bandpass	Si	0.17	–	2.0–18.4	26.5	106	Qiu et al. (2018)
RF BW scaling ring	Bandpass	Si	–	1.17–4.65	3.28–19.4	20	162.39	Xu et al. (2017)
Chip SBS	Bandpass	As2S3	–	0.02–0.04	2–12	20	520	Byrnes et al. (2012)
Ring resonator	Bandpass	Si3N4	260	–	0–12	20	46.15	Zhu et al. (2019)
Ring resonator	Notch	Si	–	0.65 -2.2	0- 25	46	–	Zheng et al. (2019)
Ring resonator	Notch	Si	0.78	–	0–40	60	–	Liu et al. (2018)
SBS on chip	Notch	As2S3	–	0.033–0.088	1–30	55	375	Marpaung et al. (2015)
Ring resonator + MZI	Band-stop	Si	–	1.85–4.55	7–34	70	–	Zhang et al. (2013)
Ring resonator	Bandpass	Si	–	0.3- 25	< 12.5	25–50	–	Jiang et al. 2018)
Ring resonator	Notch		0.78			56	48,500	Fengjie et al. (2018)
Ring resonator	Notch	Si3N4	0.78	–	1–40	60	–	Liu et al. (2018)
Ring resonator	Bandpass	Si3N4	0.072	< 0.1	0–1.4	55	–	Taddei, et al. (2014)
Ring resonator	Notch	Si3N4	–	0.15–0.3	1–12	> 50	–	Liu et al. 2017a)
Ring resonator	Bandpass	Si	–	0.67–2.8	2 -14	31.5	–	Li et al. (2019)

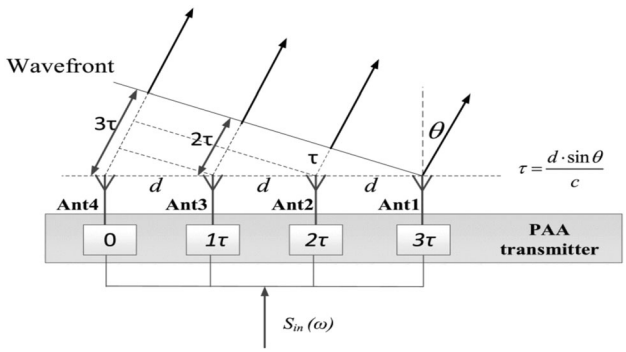

Fig. 8 Basic concept of a one-dimensional 4-element phased array transmitter (Cao et al. 2016)

respectively. To compensate this variation, the feeder network should provide no delay for Ant4, delay τ for Ant3, delay 2 τ for Ant3 and delay 3 τ for Ant1 so that all the radiated signals from all antenna elements reach at the same phase and delay at the wavefront.

The time delay τ between two successive antenna elements is given by$\tau = (d\sin\theta)/c$, where c is the speed of light in vacuum. In terms of the frequency of the input signal S_{in}, a phase shift $\varphi = \omega_s\tau = 2\pi d\sin\theta/\lambda_s$ where ω_s and λ_s are the angular frequency and wavelength of the input signal. To avoid grating lobes (undesirable multiple beams whose gain is comparable to main beam gain), the spacing d should be less than or equal to half of antenna wavelength, wavelength at which the antenna elements are designed, i.e., $d = c/(2f_a)$, then $\varphi = \pi sin\theta f_s/f_a$. For

narrow band systems, f_s=f_a, then $\varphi = \pi sin\theta$. For wideband systems, TTDs are required for beam squint-free operation since the group delays are independent of frequency as evidenced from $\tau = d\sin\theta/c$.

Making the comparison of the frequency responses of the phase shifter and TTD used in beamforming is critical. The phase response of the phase shifter is constant over the entire signal bandwidth, but its group delay response varies over the entire bandwidth. However, the phase response of ideal TDD varies linearly over entire bandwidth and its group delay is constant over entire bandwidth. The group delay variation in phase shifters causes the undesired phenomenon called beam squint effect in which different frequency components radiate toward different directions and this effect in turn causes signal distortion, degrading signal quality and SNR at the receiver. But, the ideal true-time-delay lines' phase response varies linearly over signal bandwidth and the group delay response is constant over entire bandwidth. Therefore, to combat the beam squint effect of phase shifters in broadband systems, TTDs are the best options in the beamforming networks. Figure 9 explains the effect of beam squint effect for three signals at 8 GHz, 10 GHz, and 12 GHz over a bandwidth of 4 GHz. In the phase shifter-based beamforming, the three signals radiate slightly in different directions as shown in Fig. 9a whereas all the signals radiate in the same direction as shown in Fig. 9b.

Integrated optical true-time-delay-based beamforming

Integrated electronic TTD circuits generating tunable large delay variation result in significant insertion loss at millimeter frequencies (Cao et al. 2016). For example, a typical transmission line loss in silicon is around 0.4–0.5 dB/mm at 40 GHz However, the loss for silicon-based integrated photonic waveguides is as low as 0.05 dB/mm. Moreover, delay tuning electronic circuits at millimeter frequencies are very lossy due to parasitic effect. To overcome this large insertion loss, amplification stages are required, which increases power consumption and degrades system linearity or the dynamic range. Moreover, electronic TTD circuits are designed from inductors and transmission lines and hence the footprint area is significantly large for large delay variations.

To overcome the challenges of electronic TDD circuits, photonic TTDs can provide ultra-low loss, ultra-broadband, and significantly reduced footprint. The better way to realize the TTDs is the integrated solution rather than discrete components. In discrete-based TTDs, component to component interconnection causes increased insertion loss, very poor stability, very large system size, high cost, and high-power consumption. But, integrated photonic TTDs lead to significant reduction in footprint, insertion loss, packaging cost, and power consumption. Therefore, we focus on reviewing the recent advances in integrated TTD-based beamforming. Integrated TTDs have been demonstrated most of the time using integrated optical waveguides, microring resonators, photonic crystal waveguides, and integrated Bragg grating.

Integrated optical waveguide-based TDDs

Discrete time delays can be generated by switchable TTDs under different material platforms such as in InP, silicon, and silicon nitride. Silicon nitride is the best candidate for long delay lines since it has low propagation loss as low as 0.1 dB/cm. But, InP and silicon-based optical waveguides have high propagation loss of the order of 3 dB/cm; InP has the greater loss. Integrated switched delay lines for phased array microwave photonic beamforming have been demonstrated: 3-bit in InP with curved waveguides (Soares 2006), 4-bit in Si_3N_4 with curved waveguides (Roeloffzen et al. 2018), 6-bit in Si_3N_4 with curved waveguides (Yang and Yun 2020) and 4-bit in Si_3N_4 with spiral waveguides (Taddei 2018). Figure 10 shows typical 3-bit switched TTD that can generate eight (8 = 2^3) variable time delays. Other wavelength switched arrayed waveguide (AWG)-based TTDs with re-circulating loops have been demonstrated for beamforming applications (Yeniay and Gao

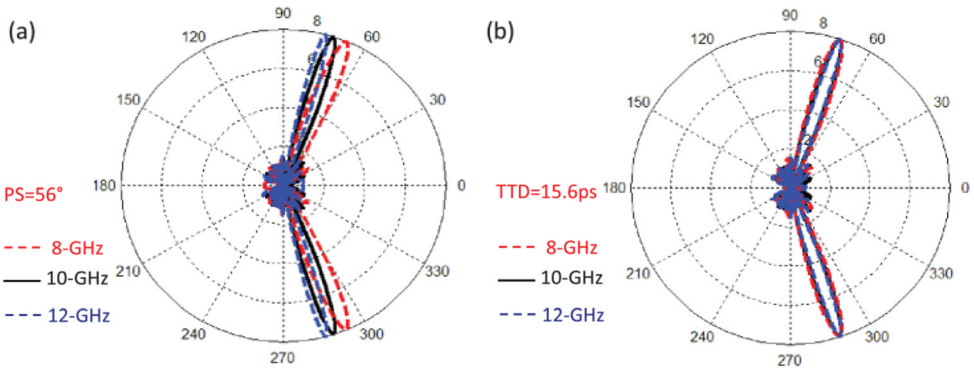

Fig. 9 Beam squint effect comparison of phase shifter-based (**a**) and TTD-based (**b**) beamforming for the frequency 8–12 GHz in a 1-by-8 array (Cao et al. 2016). © 2015 IEEE

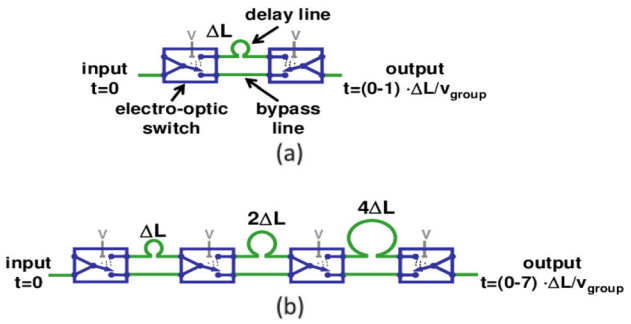

Fig. 10 Working principle of switched delay line. **a** Single switchable delay line and **b** three switchable delay lines (Soares 2006)

2010; Yegnanarayanan et al. 1996; Piqueras et al. 2006; Hu et al. 2019). The main disadvantages of switched TTDs are as follows: the limited number of discrete time delays can be generated with low delay resolution and hence limited number discrete angles can be steered, they require large physical paths for large time delay generation, and large tunable programmable switches are required leading to high-power consumption and increased physical size.

Microring resonator (MRR)-based delay lines

MRRs have attracted special attention in designing optical beamforming networks because of the following advantages: (1) compact footprint and stability, suitable for photonic integration; (2) continuous tunability and high delay resolution which means, unlike switchable TDDs, all angles within specified range can be steered or scanned; (3) complexity reduction in tuning and physical size by TDD reusability for generation of large time delays, that is, MRR can generate infinite number of delay within its bounds without changing its physical length and MRRs can be reused, for example binary-tree-structured-based beamforming (Zhuang 2010; Burla 2013).

However, the single microring resonator suffers from high group delay dispersion and narrow bandwidth. This effect manifests strongly when its coupling coefficient is tuned for high group delay, that is, increasing the time delay lowers the delay bandwidth which means the delay bandwidth and time delay product is constant (Zhuang 2010), which means increasing time delay reduces delay bandwidth and vice versa. To address the bandwidth bottleneck, two common TTD architectures are employed: side-coupled integrated spaced sequence ring resonators (SCISSORs) (Cardenas et al. 2010; Xiang et al. 2018; Khurgin and Morton 2009), as shown in Fig. 11a, where many MRRs are cascaded in series and coupled resonator optical waveguides (CROWs) (Fig. 11b), where many MRRs are coupled in series (Canciamilla et al. 2009). Cascading MRRs has two advantages, to increase the delay bandwidth and the range of the delay since delay of individual rings can be added to get larger delay values.

Wideband, continuously and thermally tunable delay lines, based on balanced SCISSORs concept, have been demonstrated on silicon-based waveguides (Cardenas et al. 2010), and low-loss silicon nitride waveguides (Xiang et al. 2018). In the first case, eight SCISSORs with the individual length of 59 μm are able to produce a bandwidth of 10 GHz and the maximum delay of 135 ps. But, the loss incurred has not been reported. In the second case, remarkable performance has been achieved using a low loss continuously tunable TTD based on single stripe Si_3N_4 waveguide with a loss less than 0.1 dB/cm. This TTD exhibits the maximum delay of 3400 ps or 3.4 ns over 10 GHz bandwidth. The length of individual racetrack microring is 7427 μm and eight SCISSORs constitute the TTD structure. In both cases, delay is tunable by adjusting the coupling coefficients and delay ripple is minimum and hence these TTDs are applicable for distortion free communication systems. Even though the footprint is very large, Si_3N_4-based TTD performances better than silicon-based TDD in high dynamic range environment since its loss is extremely low and can generate large delay. In Si TDD, to get the same delay as Si_3N_4 TDD, we can increase the length of microring resulting very high propagation loss since Si has the propagation loss of 3 dB/cm; this in turn limits dynamic range and significantly reduces the detectible power at the photodetector and the resulting RF loss is proportional to the square of optical loss. CROW-based TDDs exhibit large bandwidth, but unlike SCISSORs where single MRR has only one coupling and one phase shifter on feedback path, tunability is very challenging due to the existence of many couplings; two coupling for single MRR and one phase tuner on its the feedback path. Besides, CROWs have low fabrication tolerances. In Toroghi et al. (2016), the performance comparison has been

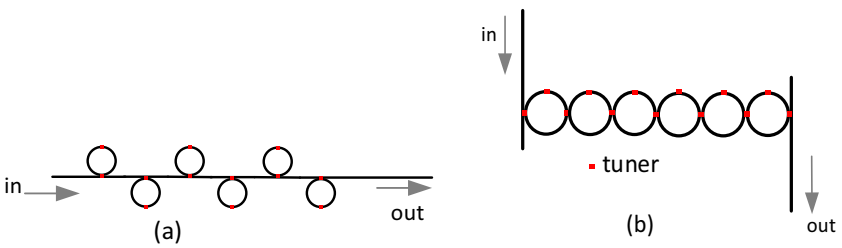

Fig. 11 Schematic of microring resonator-based delay architectures: **a** SCISSORs and **b** CROWs

carried out using different apodized grating assisted (GA) waveguide configurations of CROWs and SCISSORs. It is demonstrated that GA-SCISSORs outperformed others with the largest tunability and smallest footprint. But, the effect of power loss due to back reflection has not been reported.

In order to tackle bandwidth bottleneck and reduce tuning complexity of SCISSOR-based true-time-delay beamformers, other alternative design methods have been reported. In Mihret and Srinivas (2021, Pan et al. (2020), reflective type microring structures where two contra propagating waves are allowed to propagate there by inducing large bandwidth. The interaction of fast light and slow light produces wider bandwidth. In Mihret and Talabattula (2021 and Brunetti et al. (2018a), novel design approaches are able to increase the delay bandwidth. In the first case, the light interaction among three coupled MRRs is able produce broadband bandwidth without using SCISSORs. In the second case, designing SCISSORs to operate in anti-resonance mode has produced wideband and low delay ripple.

Integrated photonic crystal-based delay lines

Photonic crystals are two or three-dimensional periodic structures with period comparable to the optical light wavelength. The photonic bandgap theory analogous to electronic bandgap theory is a useful theory in order to predict the band of frequencies which are stopped from transmission. Because of the simpler fabrication process and low optical loss, photonic crystal slabs of high index films with two-dimensional array of air-holes surrounded by air cladding are widely used (Baba 2008). The photonic crystal waveguide is made up of a line defect of missing air-holes in photonic crystal slab. The confined light propagates through the defect due to high refractive index contrast in vertical and lateral directions. The photonic crystals exhibit large group index dispersion or group velocity dispersion in the vicinity of the photonic band edge, and hence slow or delayed light can propagate through the waveguide. By controlling this strong group index or group velocity dispersion, tunable delay lines can be designed for various applications such as in beamforming and optical buffering. There are multiple reports on delay lines based on photonic crystals: cavity based with high-quality factor (Janrao and Janyani 2015), rod like 2D photonic crystal (Kumari et al. 2021), tunable photonic crystal coupled waveguide with turnup index chirping (Adachi et al. 2008), engineered photonic crystal waveguides with low dispersion and low propagation loss (O'Faolain et al 2009). Detailed comparative review of slow-light dispersion engineered photonic crystal structures is found in Schulz et al. (2010). The main disadvantage of photonic crystals is the fabrication difficulty.

Integrated Bragg grating delay lines

This class of integrated TTD line exhibits low loss as compared to microring resonators and photonic crystal waveguides. Silicon is commonly used to design integrated Bragg grating delay lines. The principle behind this class of TTD is that silicon rib waveguide is perturbed with corrugation, for example with rectangular shape where the variation of the perturbation might be periodic, linear, or nonperiodic. Controlling of perturbation depth, width, and spacing between cycle repetitions or periods affects the transmission or reflection spectrum and the time delay performance. We can say that Bragg grating is a wavelength or frequency selective filter in which it stops or reflects band of frequencies and transmits the rest of frequency bands. So, the time delay spectrum generated depends on the wavelength bands in which the Bragg grating is designed to operate. Increasing the length of the waveguide increases the delay. The delay tuning can be carried out using plasma dispersion effect by integrating pn junction with the device or graphene-based electrodes and thermo-optic effect by integrating microheater on the top of the waveguide. In Brunetti et al. (2018b), high-performance continuously tunable graphene-based silicon Brag grating has been reported. The device achieves electro-optic switching time less than 8 ns, delay range of 200 ps, figure-of-merit of $1.54X10^5$ ps/mm^2, very low loss of 0.03 dB/ps, low power consumption of 0.05mW/ps, and bandwidth of 1.19 GHz.

In Khan and Fathpour (2012), thermally tunable TTD, with two cascaded apodized grating waveguides with complementary (positively and negatively modulated) refractive index profiles for dispersion compensation for very high data rates, has been reported. The transmission mode device achieves the following performances: loss of 5.3 dB/ns, maximum delay of 210 ps, very high bit rate of 355 Gb/s, tunability range of 90 ps, and delay and bit rate product of 75.3. Subwavelength grating enabled ultra-high compact TTD has been demonstrated Wang et al. (2016). The group delay index and consequently the time delay of TTD is controlled by changing the duty cycle of subwavelength grating. This approach solves the delay generation dependence on complex physical path variability. This approach is suitable for ultra-compact mass on-chip integration with low loss. Figure 12 illustrates simple and apodized gratings used in delay lines and other applications Ogusu (2018). However, these classes of TTDs require large waveguide length for large time delay and circulators are required to collect the reflected light, circulators make full integration impossible.

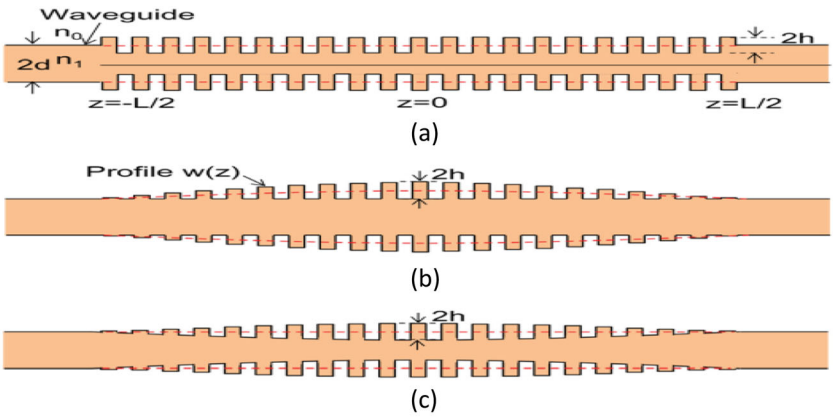

Fig. 12 Schematic of three kinds of corrugated waveguide gratings (CWG): **a** uniform CWG and **b** and **c** apodized CWGs (Ogusu 2018)

Examples of integrated optical beamforming demonstrations

In this section, we cover some breakthroughs and the state-of-the-art phased array antenna integrated beamforming implementations. Novel beamforming designs based on microring resonators have been demonstrated (Meijerink et al. 2010; Zhuang et al. 2010; Duarte et al. 2019; Marpaug et al. 2011; Marpaung et al. 2011; Morales and Monroy 2018; Liu et al. 2017c; Burla et al. 2014). The novel integrated ring resonator-based binary-tree-structured beamformer network for receive antennas was successfully analyzed theoretically and implemented experimentally in 8-by-1 linear array (Meijerink et al. 2010; Zhuang et al. 2010) as shown in Fig. 13. The core integrated components (thermally tuned passive structures) in this optical beamforming network (OBFN) are broadband delay-based ring resonators, coherent optical combiners, optical phase shifters, common optical filter for single sideband suppressed-carrier (SSSC) modulation after OBFN, carrier re-insertion coupler for balanced photodetection. The beamformer was designed for satellite television receivers. The various performance parameters, such as delay range and bandwidth of delay line, RF to RF system aspects such as loss, gain, linearity, noise, and signal-to-noise ratio (SNR), were analyzed. The results showed that the integrated OBFN is a scalable and a promising technological breakthrough for large-scale phased array antenna beamforming.

In Duarte et al. (2019), fully designed, miniaturized, scalable, modular, and coherent photonic-aided payload satellite receiver was reported. The receiver is made up of four modules: two arrays of GaAs MZM modulators, seven core erbium-doped fibers, a 4-by-1 integrated OBFN based on microrings, monitoring, and control loop for amplitude, phase, and delay stabilization. The receiver was capable of

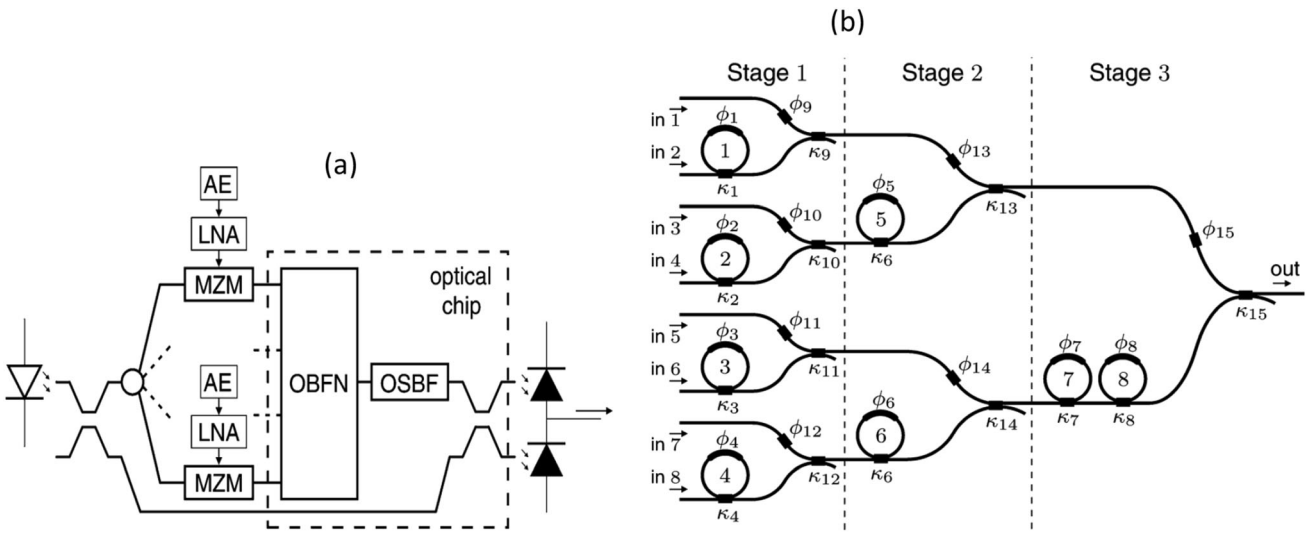

Fig. 13 **a** Ring resonator-based optical beamformer scheme. (AE: antenna element, LN: A low-noise amplifier, MZM: Mach–Zehnder modulator, OBFN: optical beamforming network, OSBF: optical sideband filter. **b** Binary-tree-based 8 1 OBFN consisting of eight optical ring resonators (ORRs) and seven combiners (Zhuang et al. 2010), © 2009 IEEE

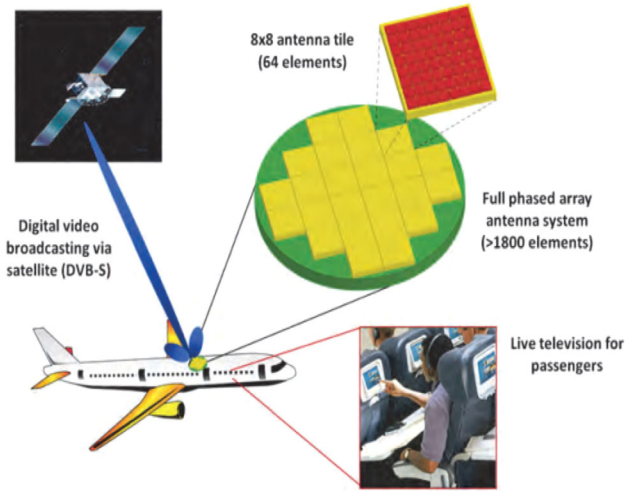

Fig. 14 Schematic description between DVB-S and airplane beamforming (Marpaug et al. 2011), © 2011 Intech

separating two beams in real time arriving from different directions. Each beam carried a 1 Gb/s quadrature phase shift keying (QPSK) signal at 28 GHz.

The ring resonator-based OBFN analyzed and designed in Meijerink et al. (2010) and Zhuang et al. (2010) was fully developed in Marpaug et al. (2011) and Marpaung et al. (2011) for airborne satellite communications in phased array antennas as shown in Fig. 14. The full system was developed in Ku-band (10.7–12.75 GHz) where digital video broadcasting satellite (DVB-S) is working. The main motive of this development was to provide passengers live television services received from a satellite. The airplane is moving at high speed and should be able track the broadcasting satellites using large-scale antenna array beamforming network as depicted in Fig. 14. The phased array antenna is composed of low aerodynamic profile 8 × 8 antenna tiles, each tile comprising 64 antenna elements (AEs). The video signal received by this phased array antenna is down-converted to L-band and then processed in OBFN. In order to tackle beamforming complexity and instability of OBFN of large antenna arrays of 2048 AEs, hybrid beamforming approach, where RF beamformers in the first stage and then OBFN in second stage, was proposed (Marpaung et al. 2011) as shown in Fig. 15. In the first stage, all outputs from 4 AEs are combined in RF beamforming network and produce 512 parallel outputs for the next stage OBFN. Then RF beamformed outputs are fed to 32 number of 16 × 1 OBFNs. Each of 16 × 1 OBFN output is converted back to RF by balanced photodetector. All parallel 32 RF outputs are again modulated by the laser and fed to the next two parallel 16 × 1 OBFNs and the then outputs from two 16 × 1 OBFN are summed to produce the overall output of the beamformer system. In order to mitigate high pass loss of millimeter-wave frequencies, the silicon nitride integrated 1-by-4 binary-tree-structured OBFN for millimeter-wave frequencies of 60 GHz (Morales and Monroy 2018) and W-band 80 GHz (Liu et al. 2018) were designed for transmitter phased array antenna. In Liu et al. (2017c), the tuning optimization has been done for flattened bandwidth of 6 GHz and dynamic delay tuning range of 209 ps, and the result shows the suitability for high-frequency millimeter-wave data rate communications.

A novel hardware compressive, for compact footprint and complexity reduction, continuously tunable OBFN based on microring resonators was demonstrated for receiver phased array antennas (Burla et al. 2014). This novel idea utilizes the periodic response of SCISSORs and wavelength division multiplexing in order to transmit multiple signals on a single delay channel. The concept is illustrated in Fig. 16 for two-dimensional 4 × 4 phased array antennas. As shown in Fig. 16a, the beamforming is carried out in horizontal-y direction and then along vertical x-direction. All antenna elements aligned columnize along y-horizontal direction, (1,1),(1,2),(1,3),(1,4);(2,1), (2,2),(2,3),(2,4); (3,1), (3,2),(3,4);(4,1), (4,2), (4,3),(4,4), have the same progressive time delay (τ_y,$2\tau_y$,$3\tau_y$,$4\tau_y$), but each successive row differs by time delay of τ_x along x vertical direction forming linear progressive delay of (τ_x,$2\tau_x$,$3\tau_x$,$4\tau_x$). Therefore, the horizontal combining of every row needs identical delay structure as indicated by numbers 1,2,3, and 4 in Fig. 16a. In the horizontal combining, every row has four input paths and each path has different delays. The corresponding paths of all rows have identical delays D_1, D_2, D_3, and D_4. Paths with D_1:(1,1), (2,1), (3,1), (4,1); paths with D_2:(1,2), (2,2), (3,2), (4,2); paths with D_3:(1,3), (2,3), (3,3), (4,3): paths with D_4: (1,4), (2,4), (3,4), (4,4). Instead of using four identical parallel structures for every row, one common structure is utilized by multiplexing each path with the same delay in four different wavelengths λ_1, λ_2, λ_3, and λ_4 as shown in Fig. 16b. For vertical combining along x-direction, the same delay structure used in horizontal combining is utilized after demultiplexing where each delay path from horizontal combining goes to the corresponding path in vertical combining. Figure 16c shows detailed connection of antenna arrays and four wavelength multiplexers whose outputs are going to be fed to OBFN.

Suppose NxN square matrix of 2D-antenna arrays where N is a power of 2 and a single ring resonator is sufficient to produce the desired differential delay between adjacent antenna elements (AEs). The total number of optical microring resonators (ORRs) in conventional single wavelength beamforming is $ORR_{SWL} = (N+1)(0.5*N)log\log_2 N$ which is in the order of $O(N^2 log\log_2 N)$ and the number of ORRs required in multiwavelength beamforming is $ORR_{MWL} =$

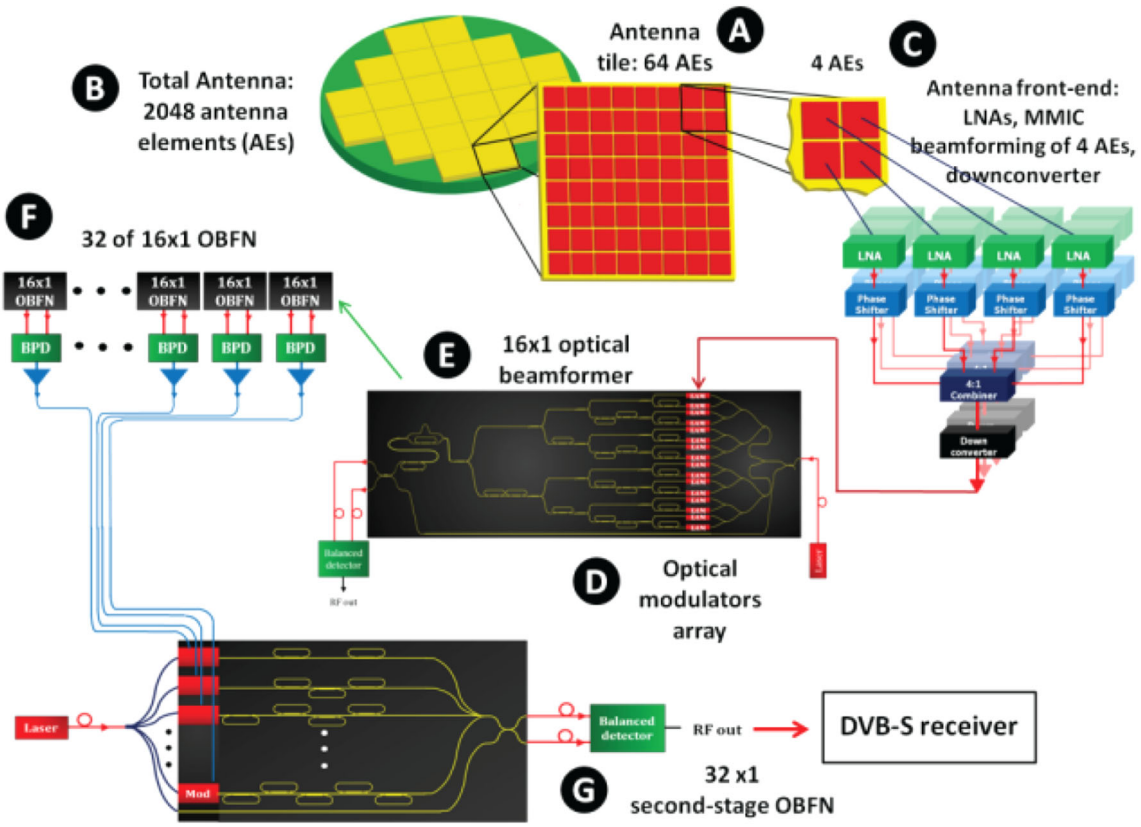

Fig. 15 **a** An antenna tile consisting of 64 elements, **b** total 2048 AEs, **c** the RF front-end consisting of LNAs, MMIC phase shifter, a 4-to-1 combiner and a downconverter, **d** an array of optical modulator integrated with a 16 × 1 optical beamformer, **e** Thirty-two 16 × 1 beamforming RF outputs, **f** all 32 number RF outputs combined/beamformed in second stage with OBFN **g**. BPD: balanced photodetector (Marpaung et al. 2011), © 2011 IEEE

$2(0.5N)log\log_2 N$ which is in the order of $O(N\log_2 N)$. This dramatic reduction in complexity can be easily observed in Fig. 17. For example, for N = 16, $ORR_{SWL} = 544$, $ORR_{MWL} = 64$, and at the same time the required number of heaters and combining couplers also reduce dramatically.

A 1-by-8 (1 × 8) monolithically integrated SOI microwave photonic beamformer based on a 5-bit switchable TTDs has been reported (Zhu et al. 2020), as illustrated in Fig. 18. Each delay stage is formed by two switches and two unequal length waveguides, the longer for delay generation and the shorter for reference, between the two switches. The high-speed optical modulators and photodetectors are integrated with OBFN. The time delay is generated by digitally switching to the longer or the shorter waveguide. The differential delay for each stage is $2^n\Delta t$, where n = 1,2,3,4,5, and Δt is the smallest delay resolution that can be generated. Since there are five delay stages, 32 or 2^5 number of time delays can be generated thereby steering 32 number of angles from − 75.51° to 75.64°. The fully integrated, except laser source, OBFN has a compact footprint of 11.03 × 3.88 mm^2, a bandwidth of 10 GHz, non-continuous delay tuning range from 0 to 496 ps, power and power consumption of 1450 mW, and beam steering range of − 75.51° to 75.64°. Besides, the OBFN chip is driven by electro-optic effect with fast time response of 56 µs. The successfully implemented integrated microwave photonic beamformer has showed a great potential in miniaturized radar and broadband communication systems. However, the beamformer covers limited and discrete set of angles, it is not continuously tunable.

OBFNs based on wavelength selective TTDs have been demonstrated in Yeniay and Gao (2010), Yegnanarayanan et al. (1996), Piqueras et al. (2006), and Hu et al. (2019). The NxN arrayed waveguide (AWG) takes N number of input wavelengths and multiplexes them, at the output it demultiplexes them at N number of its outputs. When AWG is used as TTDs for beamforming, as shown in Fig. 19, the N-1 outputs are looped back/connected to the N-1 inputs through delay lines with progressive lengths; one channel is used as input for multiplexed signals and one channel is used as an output for N-1 time delayed multiplexed signals and another AWG demultiplexes into the antenna elements. The advanced and recently reported AWG-based OBFN has the capability to steer multiple

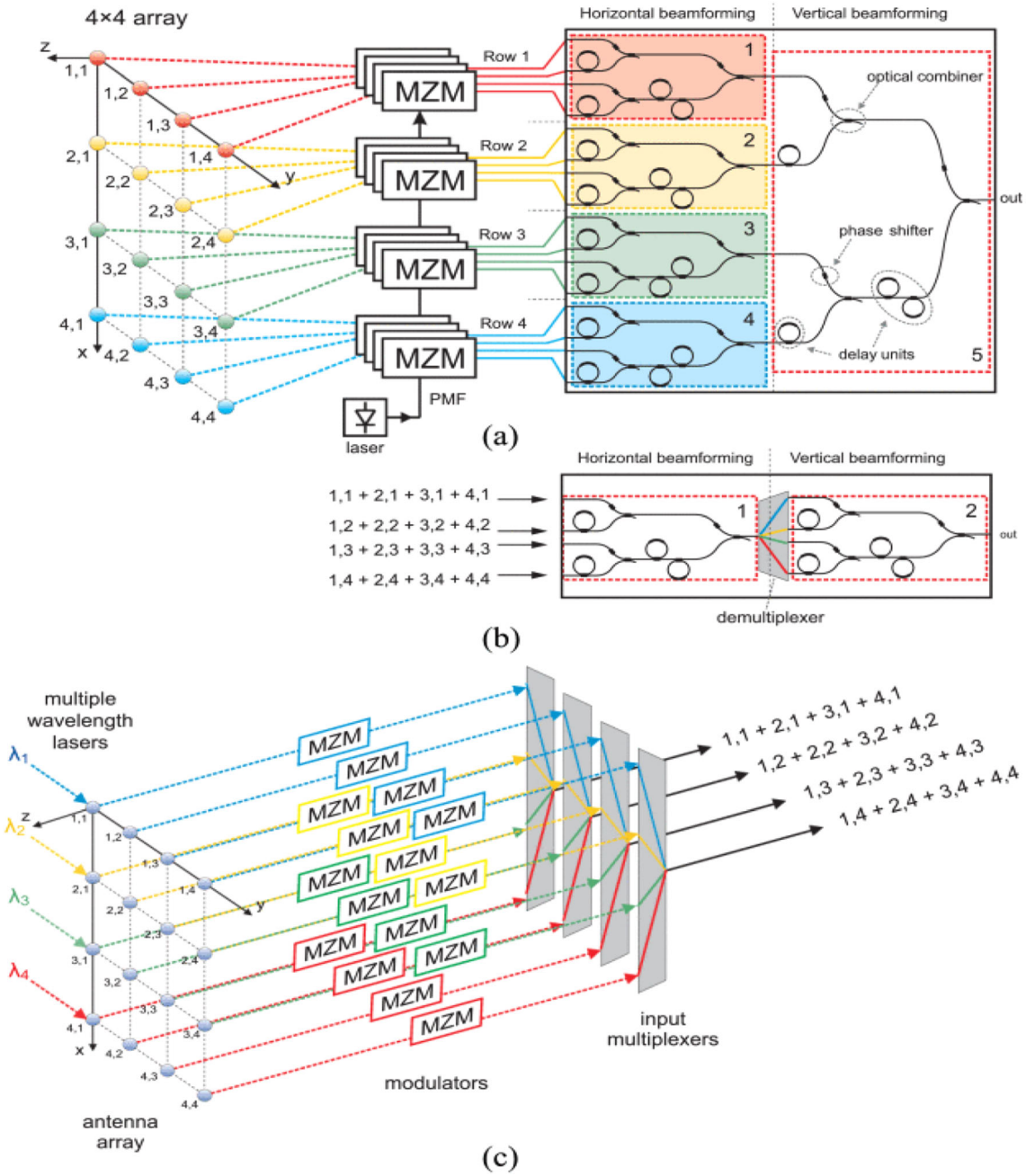

Fig. 16 Schematic of horizontal and vertical combing of 4 × 4 array (**a**) and detailed structure (**b**). Complexity reduction using multi-wavelength concept. Detailed connection of antenna arrays and four wavelength multiplexers whose outputs are going to be fed to OBFN (**c**) (Burla et al. 2014), © 2014 IEEE

beams simultaneously (Hu et al. 2019), as illustrated in Fig. 20.

As we see from the schematic of Fig. 20b, the integrated beamformer consists of phased array antenna with eight elements (element 1, element2…. element8), 23 × 23 AWG for dense wavelength multiplexing (DWDM) with 22 looped-back TTDs, and 1 × 8 AWG for coarse wavelength division wavelength (CWDM). A set of AWG input wavelengths (λ_1,λ_2,…, λ_{22}) are selectively diffracted to the corresponding looped-back TTDs, each wavelength is diffracted to unique TTD. The same set of wavelengths are diffracted to the same TTDs after a diffraction order of 2 π since the response of AWG is periodic, that is, at the integer multiple of frequency spacing between successive periods (free spectral range, λ_{FSR}), the response is same. Therefore, the set of wavelengths (λ_1,λ_2,…, λ_{22}) can be shifted by λ_{FSR},2λ_{FSR}, 3λ_{FSR},…, 7λ_{FSR} forming another set of wave lengths $\{\lambda_I, \lambda_{II}, \ldots \lambda_{VIII}\} = \{ \lambda_{FSR} + (\lambda_1,\lambda_2,\ldots,$

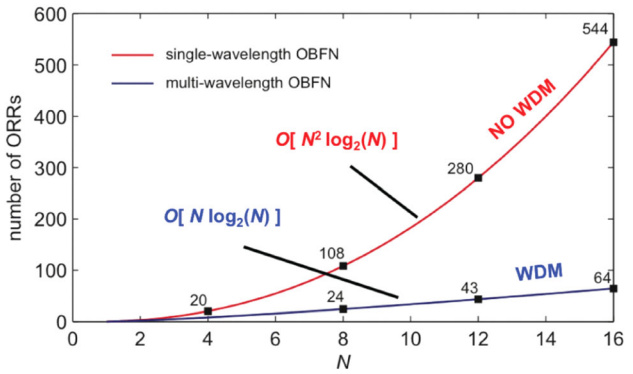

Fig. 17 The number of ORRs vs antenna array dimension, N. WDM: wavelength division multiplexing, NO WDM: without WDM (Burla et al. 2014) © 2014 IEEE

$\lambda_{22})$, $2\lambda_{FSR} + (\lambda_1,\lambda_2,\ldots,\lambda_{22}),\ldots, 7\lambda_{FSR} + (\lambda_1,\lambda_2,\ldots,\lambda_{22})\}$. Signals passing through same TTD achieve the same simultaneous time delays. These set of frequencies, $\{\lambda_I, \lambda_{II}, \ldots \lambda_{VIII}\}$, corresponding to inputs to the eight antenna elements, as shown in Fig. 20b, would be separated or demultiplexed by 1 × 8 AWG, and then fed to the photodetectors to be converted to RF domain and applied to array antenna for radiation. The OBFN was fabricated using germanium doped silica waveguide on silicon substrate for low propagation loss and low chip to fiber coupling loss. The fabricated beamformer delay range is from 0 to 278 ps in 5.7 ps increments of eight diffraction orders. The measured insertion loss is less than 1.5 dB over 1527 to 1607 nm wavelength range. The main disadvantage of this beamformer is the limited scanning angles and the use of two complex of AWGs.

Integrated microwave photonic signal generation

The generation of low-noise broadband microwave and millimeter-wave frequency signals is vital in applications including radar systems (Ghelfi et al. 2014; Pan and Zhang

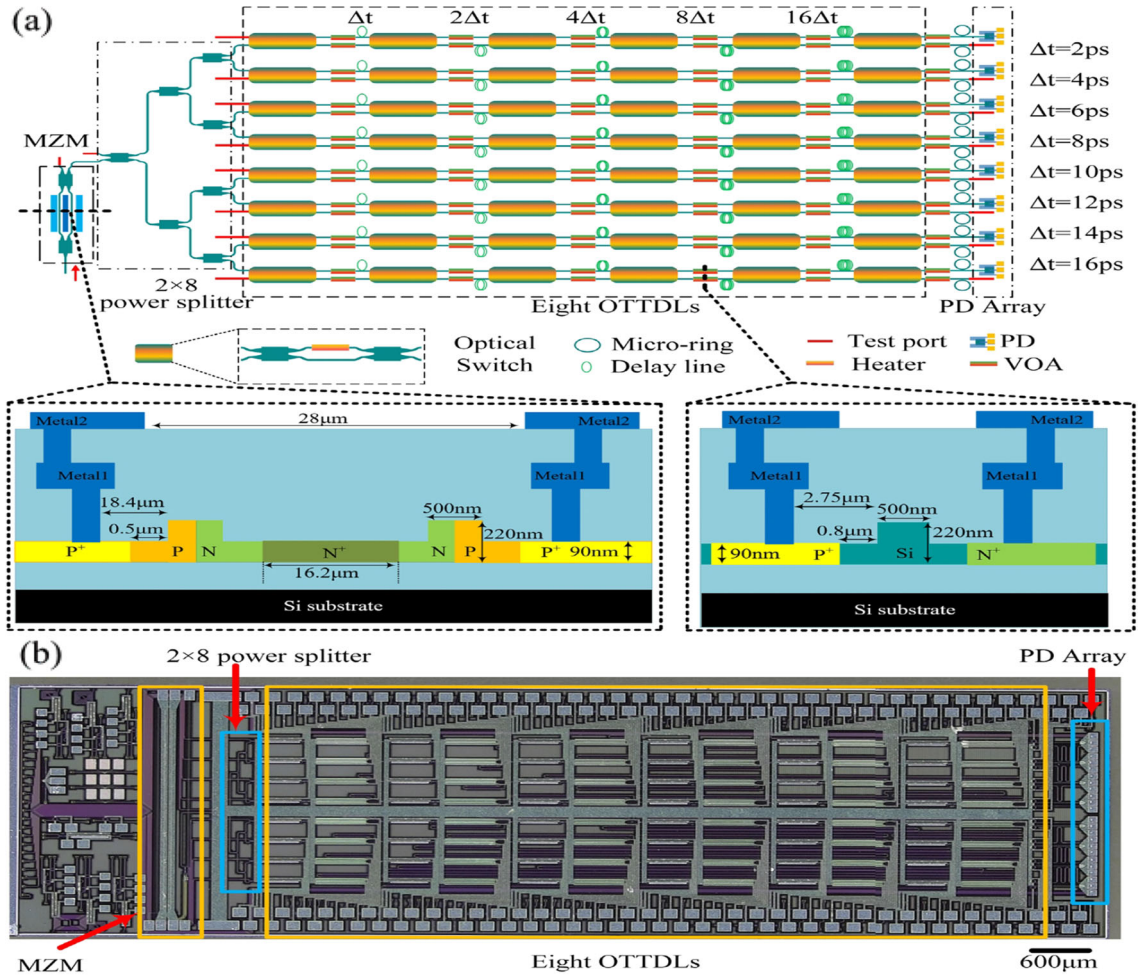

Fig. 18 **a** Schematic of the 1 × 8 microwave phased array chip. The insets are the cross-sections of the MZM and VOA. **b** Microscope image of the fabricated chip (Zhu et al. 2020) 2020, © OSA, Optica

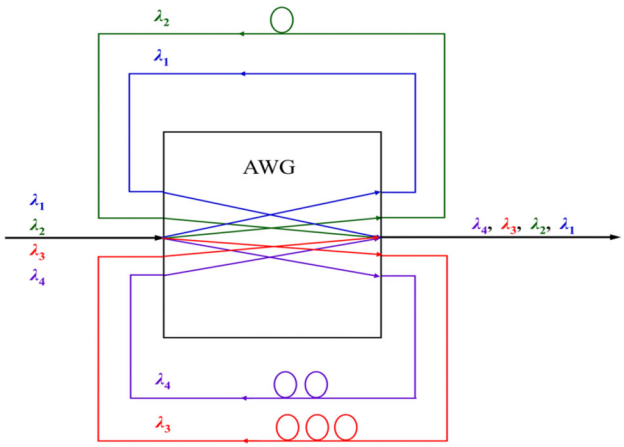

Fig. 19 **a** Wavelength selective OTTD module based on AWG in loop-back configuration (Hu et al. 2019)

2020b), wireless communication systems (Balakier et al. 2020), and warfare systems (Manka 2008), frequency identification (Burla et al. 2016). The traditional approach to generate microwave and millimeter-wave frequencies based on discrete optical devices, and fiber-based components increases cost and size, and lacks flexibility and stability. The integrated approach solves these problems. The two approaches, suitable for the integration process in generating microwave and millimeter-wave frequencies, are optical heterodyning and optical mode locking (Carpintero et al. 2016). Optical heterodyning requires two optical wavelength sources separated by a wavelength spacing $\Delta\lambda = \lambda_1 - \lambda_2$, optical coupler for combing these sources, photodetector to produce the electrical signal with beat frequency note f_0 which is dictated by the spacing $\Delta\lambda$ and absolute product values $\lambda_1\lambda_2$ as, $f_0 = c\Delta\lambda/(\lambda_1\lambda_2)$, where c is the speed of light in vacuum as illustrated in Fig. 21a. To take the advantage of integration, two tunable laser diodes based on distributed feedback lasers can be employed to generate tunable beat note frequency f_0. The main drawback of heterodyning is that the two lasers are non-coherent and are susceptible to uncorrelated phase-noise which leads to instability of the beat frequency. To tackle this problem, phase-locking techniques such as single optical carrier modulated with fractional or integer multiples of frequency f_0, optical frequency comb generator (OFCG) and optical phase-locked loop (OPLL) can be applied (Wang et al. 2015). In the first case, MZM-based intensity modulator, biased at its minimum transmission point, modulates a microwave signal of frequency ($f_0/2$) with an optical carrier of frequency f_c, resulting two sidebands with suppressed carrier. The two sidebands spaced f_0 apart, ($f_c + f_0/2$-(-f_c-f_0/2) = f_0), are applied to the photodetector producing an RF signal of frequency f_0. In the

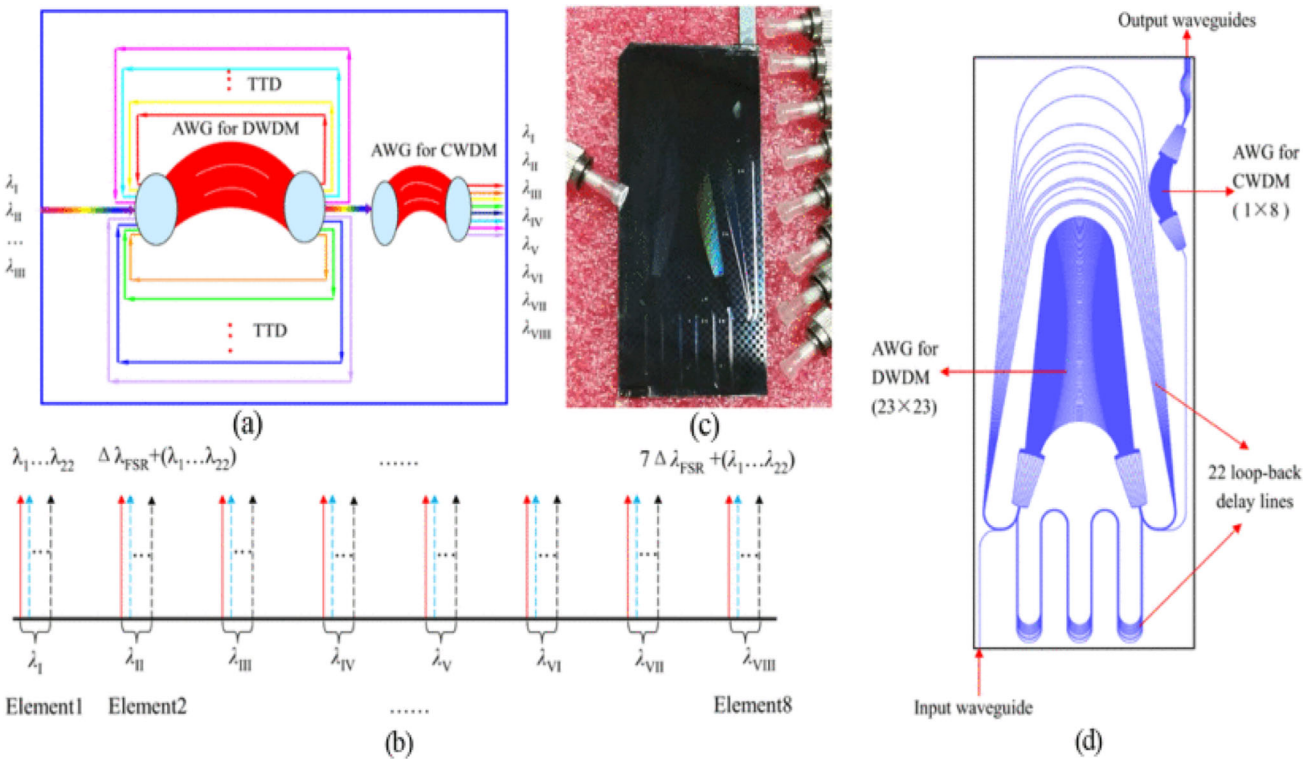

Fig. 20 The architecture of monolithic integration of the optical beamformer. **a** Schematics of the architecture. **b** The relation between the signal wavelengths and the eight antenna elements. **c** The fabricated integrated beamformer. **d** Mask layout of the fabricated integrated beamformer (Hu et al. 2019), © 2019 IEEE

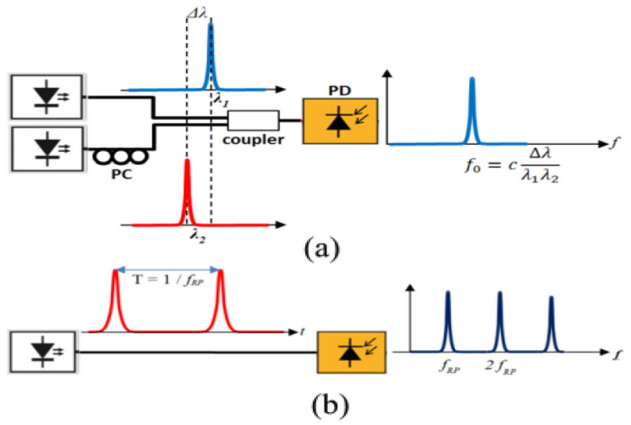

Fig. 21 Photonic-based signal generation techniques: **a** optical heterodyne of two slightly different optical wavelengths and **b** single pulsed source generating optical pulses spaced by the inverse of the repetition rate with the generated electrical spectrum on a PD. PC: polarization controller (Carpintero et al. 2016)

second case, an optical filter, for example microring resonator-based filter with Signac reflector (Jiayang et al. 2015), to select two comb frequencies which align with the two passband frequencies of the filter, that is, the filter's spectral range is the same as the spacing of the frequency combs. Besides, a wideband and continuously tunable microwave signal generator was reported in Do et al. (2020). The device architecture is made of a single passband microring resonator (designed as a drop filter), MZM modulator and photodetector and RF coupler. The input optical power is split into two, one is used as reference for heterodyning at photodetector and the other is fed to ring resonator. The output of a ring resonator and reference signal are combined and fed to the photodetector resulting in an RF signal whose frequency is the difference between ring resonator's passband resonance frequency and the reference signal frequency. Then some percentage of RF power is fed to the modulator for the reconfigurable RF frequency generation from 6 to 18 GHz.

The second approach of generating microwave signals is using monolithically integrated mode-locked lasers (MLL) which generate coherent and stable uniformly spaced frequency lines. Integrating photodiode to the MLL, periodic microwave signals with spacing equivalent to the spacing of MLL comb frequencies as illustrated in Fig. 21b can be generated. If the spacing of comb lines is f_{RP}, then the microwave signals with f_{RP}, $2f_{RP}$, $3f_{RP}$, and so on will be generated limited by the bandwidth of the photodetector. Under this category, advanced ultra-broadband and reconfigurable arbitrary microwave signal generation on-chip silicon photonics were demonstrated (Wang et al. 2015; Khan et al. 2009). The spectral reconfigurability has been carried out by thermal or electro-optic tuning of the cascaded microrings, eight as drop filters (Wang et al. 2015) and two-stage eight drop filters with delay lines in between them (Khan et al. 2009).

Challenges and prospects

Even though integrated photonics has played a significant role in designing ultra-broadband, low loss, programmable and compact devices in RF/microwave signal processing for wireless systems, it may pose challenges from implementation point of view. Firstly, RF performances such as insertion loss, gain, noise figure, and linearity should be taken into considerations. RF power output, which is the output of photodetector after optical signal processor, is proportional to the square of the optical power incident into the photodetector. If the photonic processing introduces large loss, including modulator insertion loss relatively high as compared to photonic processor loss, RF power loss is proportional to the square of optical power loss. This loss reduces the overall RF gain and limits the operating spurious dynamic range (SFDR) of the system. The nonlinearity introduced by modulators, photodetectors and photonic processors and materials also causes distortion to the information signal, making decoding challenging at the receiver. Even if many researchers have been conducting to alleviate the problems, there are always performance tradeoffs, that is, when one performance is improved, the other performance is compromised.

Secondly, the complexity of photonic processing increases with some applications, for example photonic beamforming. In optical beamforming of phased large array antennas, maintaining squint-free operation, low loss, speed of reconfigurability (in order of microseconds), multibeam capability is challenging. The use of true-time-delay lines avoids beam squint, but the complexity scales dramatically with large array antennas. For steering beam continuously over a predefined angular range, reconfigurable TTDs are required and tuning complexity scales with increased number of TTDs for example in binary-structured ring resonator-based beamforming. Besides, thermo-optic tuners introduce thermal cross-talk and are very slow while electro-optic tuners introduce large loss even though they exhibit fast response time for programmability.

Thirdly, photonic processors under different material technologies have been designed by various researchers globally to address the performance issues. For example, to reduce insertion loss silicon nitride material platform is an ideal solution and hence silicon nitride-based microwave photonic filters and beamformers are common these days. To reduce footprint and allow seamless integration with matured CMOS foundry, silicon material is attracting attention even though it introduces large loss and has poor

power handling (cannot carry large power to compensate loss since nonlinearity arises at high power). Moreover, for high spectral resolution filtering the nonlinear effect of stimulated Brillouin scattering (SBS)-based chalcogenide materials are employed, and for active modulators and photodetectors GaAs and InP material platforms are required. So, integrating all different material platforms into one integration is a challenging and it is active area of research.

Finally, designing application specific photonic processors is time-consuming and expensive. It is vital to develop the general-purpose programmable processors that can be reconfigured or programmed for multiple functionalities. For instance, a single large-scale programmable photonic integrated chip can be reconfigured to function as microwave photonic filter and as photonic optical beamformer. Even though there are few demonstrations in this decade, the development of versatile general-purpose photonic processors is in infant stage and it is under active research.

References

Abdalla AM, Rodriguez J, Texeir A (2019) Optical and wireless convergence for 5G networks. IEEE Press, Wiley

Adachi J, Ishikura N, Sasaki H, Baba T (2008) Record wide range tuning of slow light pulse in photonic crystal coupled waveguide via turnup chirping. Advances in Optical Sciences Congress, OSA Technical Digest 1:1. https://doi.org/10.1364/SL.2009.SWA1

Baba T (2008) Slow light in photonic crystals. Nat Photon. https://doi.org/10.1038/nphoton.2008.146

Balakier K et al (2020) Integrated photonics for wireless and satellite applications. OSA Adv Photon Congr. https://doi.org/10.1364/NETWORKS.2020.NeTu3B.2

Boyd RW (2008) Nonlinear Optics, 3rd edn. Academic Press, Burlington, VT

Boynton N et al (2020) A heterogeneously integrated silicon photonic/lithium niobate travelling wave electro-optic modulator. Opt Express 1:1. https://doi.org/10.1364/OE.28.001868

Brunetti G et al (2018a) Design of an ultra-compact graphene-based integrated microphotonic tunable delay line. Opt Express 1:1. https://doi.org/10.1364/OE.26.004593

Brunetti G et al (2018b) Design of an ultra-compact graphene-based integrated microphotonic tunable delay line. Opt Express. https://doi.org/10.1364/OE.26.004593

Burla M (2013) Advanced integrated optical beam forming networks for broadband phased array antenna systems. Dissertation, University of Twente. https://doi.org/10.3990/1.9789036507295

Burla M et al (2014) Multiwavelength-integrated optical beamformer based on wavelength division multiplexing for 2-D phased array antennas. J Lightwave Technol. https://doi.org/10.1109/JLT.2014.2332426

Burla M, Wang X, Li M et al (2016) Wideband dynamic microwave frequency identification system using a low-power ultracompact silicon photonic chip. Nat Commun https://doi.org/10.1038/ncomms13004.

Burla M et al (2019) 500 GHz plasmonic Mach-Zehnder modulator enabling sub-THz microwave photonics. APL Photon. https://doi.org/10.1063/1.5086868.

Byrnes A et al (2012) Photonic chip based tunable and reconfigurable narrowband microwave photonic filter using stimulated Brillouin scattering. Opt Express. https://doi.org/10.1364/OE.20.018836

Canciamilla A et al (2009) Reconfigurable CROW delay lines on a silicon platform. Cleo/Europe - EQEC. https://doi.org/10.1109/CLEOE-EQEC.2009.5192032

Cao Z et al (2016) Advanced integration techniques on broadband millimeter-wave beam steering for 5G wireless networks and beyond. IEEE J Quantum Electron. https://doi.org/10.1109/JQE.2015.2509256

Cardenas J et al (2010) Wide-bandwidth continuously tunable optical delay line using silicon microring resonators. Opt Express. https://doi.org/10.1364/OE.18.026525

Carpintero G et al (2016) Photonic integrated circuits for radio-frequency signal generation. J Lightwave Technol. https://doi.org/10.1109/JLT.2015.2511040

Chang L et al (2021) Second order nonlinear photonic integrated platforms for optical signal processing. IEEE J Sel Top Quantum Electron. https://doi.org/10.1109/JSTQE.2020.3025219

Chen L, Chen J, Nagy J, Reano RM (2015) Highly linear ring modulator from hybrid silicon and lithium niobate. Opt Express 1:1. https://doi.org/10.1364/OE.23.013255

Del'Haye P, Schliesser A, Arcizet O et al (2007) Optical frequency comb generation from a monolithic microresonator. Nature. https://doi.org/10.1038/nature06401

Do PT, Alonso-Ramos C, Le Roux X et al (2020) Wideband tunable microwave signal generation in a silicon-micro-ring-based optoelectronic oscillator. Sci Rep. https://doi.org/10.1038/s41598-020-63414-9

Dong P, Xie C, Chen L, Buhl LL, Chen Y (2012) 112-Gb/s monolithic PDM-QPSK modulator in silicon. European Conference and Exhibition on Optical Communication, OSA Technical Digest. https://doi.org/10.1364/OE.20.00B624

Dong P, Xie C, Buhl LL, Chen Y (2013) Silicon microring modulators for advanced modulation formats. Optical Fiber Communication, OSA. https://doi.org/10.1364/OFC.2013.OW4J.2

Duarte VC, Prata JG, Ribeiro CF et al (2019) Modular coherent photonic-aided payload receiver for communications satellites. Nat Commun.https://doi.org/10.1038/s41467-019-10077-4.

Fengjie Z, Gu X, Kong Y, Niu B, Qian G (2018) A tunable microwave-photonic notch filter based on single silicon ring resonator. ACP. https://doi.org/10.1109/ACP.2018.8596063

Ghelfi P, Laghezza F, Scotti F et al (2014) A fully photonics-based coherent radar system. Nature. https://doi.org/10.1038/nature13078

Hu G et al (2019) Optical beamformer based on diffraction order multiplexing (DOM) of an arrayed waveguide grating. J Lightwave Technol. https://doi.org/10.1109/JLT.2019.2904710

Janrao N, Janyani V (2015) Slow light photonic crystal waveguide with large quality factor. Optik. https://doi.org/10.1016/j.ijleo.2015.11.015

Jiang H, Yan L, Marpaung D et al (2018) Chip-based arbitrary radio-frequency photonic filter with algorithm-driven reconfigurable resolution. Opt Lett. https://doi.org/10.1364/OL.43.000415

Jiayang Wu et al (2015) Passive silicon photonic devices for microwave photonic signal processing. Opt Commun. https://doi.org/10.1016/j.optcom.2015.07.045

Jin W et al (2017) Piezoelectric tuning of a suspended silicon nitride ring resonator. IEEE Photon Conf (IPC). https://doi.org/10.1109/IPCon.2017.8116029

Khan S, Fathpour S (2012) Complementary apodized grating waveguides for tunable optical delay lines. Opt Express. https://doi.org/10.1364/OE.20.019859

Khan M, Shen H, Xuan Y et al (2009) Ultrabroad-bandwidth arbitrary radiofrequency waveform generation with a silicon photonic chip-based spectral shaper. Nature Photon. https://doi.org/10.1038/nphoton.2009.266

Khurgin JB, Morton PA (2009) Tunable wideband optical delay line based on balanced coupled resonator structures. Opt Lett. https://doi.org/10.1364/OL.34.002655

Komljenovic T et al (2016) Heterogeneous Silicon Photonic Integrated Circuits. J Lightwave Technol. https://doi.org/10.1109/JLT.2015.2465382

Kuar P et al (2021) Hybrid and heterogeneous photonic integration. APL Photon Doi 10(1063/5):0052700

Kumari S, Kumar A, Medhekar S (2021) Slow light in rod type 2D photonic crystal waveguide comprising of cavity: optimization and analysis. Optik 1:1. https://doi.org/10.1016/j.ijleo.2021.166438

Kuo Y et al (2006) Quantum-confined stark effect in Ge/SiGe quantum wells on Si for optical modulators. IEEE J Sel Top Quantum Electron 1:1. https://doi.org/10.1109/JSTQE.2006.883146

Langrock C, et al. (2006) All-optical Signal Processing Using $\chi^{(2)}$ Nonlinearities in Guided-Wave Devices. J Lightwave Technol. https://doi.org/10.1109/JLT.2006.874605

Lauermann M et al (2014) Low-power silicon-organic hybrid (SOH) modulators for advanced modulation formats. Opt Express. https://doi.org/10.1364/OE.22.029927

Lauermann M et al (2016) Generation of 64 GBd 4ASK signals using a silicon-organic hybrid modulator at 80°C. Opt Express. https://doi.org/10.1364/OE.24.009389

Lee CH (2006) Microwave photonics. Tylor and Francis

Li J et al (2019) Performance improvements of a tunable bandpass microwave photonic filter based on a notch ring resonator using phase modulation with dual optical carriers. Opt Express. https://doi.org/10.1364/OE.27.009705

Li G et al (2021) Microresonator-based optical frequency combs. Science. https://doi.org/10.1126/sciadv.abe4335

Liu Y et al (2017b) All-optimized integrated RF photonic notch filter. Opt Lett. https://doi.org/10.1364/OL.42.004631

Liu Y et al (2017c) Tuning optimization of ring resonator delays for integrated optical beam forming networks. J Lightwave Technol. https://doi.org/10.1109/JLT.2017.2762641

Liu X et al (2018) Silicon-on-insulator-based microwave photonic filter with narrowband and ultrahigh peak rejection. Opt Lett. https://doi.org/10.1364/OL.43.001359

Liu Y, Marpaung D, Choudhary A and Eggleton BJ (2017a) Highly selective and reconfigurable Si3N4 RF photonic notch filter with negligible RF losses. Conference on Lasers and Electro-Optics (CLEO)

Manka ME (2008) Microwave photonics for Electronic Warfare applications. International Topical Meeting on Microwave Photonics jointly held with the 2008 Asia-Pacific Microwave Photonics Conference. https://doi.org/10.1109/MWP.2008.4666690.

Marpaug D et al (2011) Development of a broadband and squint-free Ku-band phased array antenna system for airborne satellite communications. INTECH. https://doi.org/10.5772/28399

Marpaung D, Morrison B, Pagani M, Pant R, Choi D-Y, Luther-Davies B, Madden SJ, Eggleton BJ (2015) Low-power, chip-based stimulated Brillouin scattering microwave photonic filter with ultrahigh selectivity. Optica. https://doi.org/10.1364/OPTICA.2.000076

Marpaung D, Yao J, Capmany J (2019) Integrated microwave photonics. Nature Photon. https://doi.org/10.1038/s41566-018-0310-5

Marpaung D et al. (2011) Towards a broadband and squint-free Ku-band phased array antenna system for airborne satellite communications. Proceedings of the 5th European Conference on Antennas and Propagation.

Marpaung D et al. (2014) Ultrahigh suppression and reconfigurable RF photonic notch filter using a silicon nitride ring resonator .CLEO: 2014, OSA . https://doi.org/10.1364/CLEO_SI.2014.SF2O.1 .

Meijerink A et al (2010) Novel ring resonator-based integrated photonic beamformer for broadband phased array receive antennas—part i: design and performance analysis. J Lightwave Technol. https://doi.org/10.1109/JLT.2009.2029705

Mihret F, Kumar P and Srinivas T (2020) Hybrid photonic beamforming for 5G downlink millimeter wave MIMO communication. In: IEEE international conference on electronics, computing and communication technologies (CONECCT. https://doi.org/10.1109/CONECCT50063.2020.9198561

Mihret F, Srinivas T (2021) Reflective coupled microring resonators for reconfigurable photonic systems: Performance analysis. Results in Optics. https://doi.org/10.1016/j.rio.2021.100111

Mihret F, Talabattula S (2021) Performance analysis of reconfigurable multifunctional photonic filters using triple coupled microring resonators. Opt Commun 1:1. https://doi.org/10.1016/j.optcom.2021.126800

Morales A, Monroy IT (2018) Silicon nitride integrated optical beamforming network for millimeter wave photonics systems. European Microwave Conference (EuMC). https://doi.org/10.23919/EuMC.2018.8541583

Nazoki K et al (2017) Ultralow-energy electro-absorption modulator consisting of InGaAsP-embedded photonic-crystal waveguide. APL Photon 1:1. https://doi.org/10.1063/1.4980036

Nedeljkovic M, Soref R, Mashanovich GZ (2011) Free-carrier electrorefraction and electroabsorption modulation predictions for silicon over the 1–14um infrared wavelength range. IEEE Photon J 1:1. https://doi.org/10.1109/JPHOT.2011.2171930

Norris B, Bland-Hawthorn J (2019) Astrophotonics: The rise of integrated photonics in astronomy. Opt Photonics News 30(5):26–33. https://doi.org/10.1364/OPN.30.5.000026

O'Faolain L et al (2009) Low loss dispersion engineered photonic crystal waveguides for optical delay lines. 6th IEEE International Conference on Group IV Photonics. https://doi.org/10.1109/GROUP4.2009.5338297.

Ogusu K (2018) Simple apodization technique for surface-corrugated waveguide gratings. Opt Commun. https://doi.org/10.1016/j.optcom.2018.06.055

Pan S, Tang Z, Huang M and Li S (2020) Reflective-type microring resonator for on-chip reconfigurable microwave photonic systems. IEEE J Sel Top Quant Electron. https://doi.org/10.1109/JSTQE.2020.2969567.

Pan S, Zhang Y (2020a) Microwave photonic radars. IEEE J Lightw Technol 38(19):1. https://doi.org/10.1109/JLT.2020a.2993166

Pan S, Zhang Y (2020b) Microwave Photonic Radars. J Lightwave Technol. https://doi.org/10.1109/JLT.2020.2993166

Pérez D, Gasulla I, Capmany J (2018) Programmable multifunctional integrated nanophotonics. Nanophotonics https://doi.org/10.1515/nanoph-2018-0051.

Piqueras MA et al (2006) Optically beamformed beam-switched adaptive antennas for fixed and mobile broad-band wireless access networks. IEEE Trans Microw Theory Tech. https://doi.org/10.1109/TMTT.2005.863049

Preetpaul Singh Devgan (2018) Applications of modern RF photonics. Artech House, London

Qiu H et al (2018) A continuously tunable sub-gigahertz microwave photonic bandpass filter based on an ultra-high-Q silicon microring resonator. J Lightwave Technol. https://doi.org/10.1109/JLT.2018.2822829

Roeloffzen CGH et al (2018) Low-Loss Si3N4 TriPleX Optical Waveguides: Technology and Applications Overview. IEEE J Sel Top Quantum Electron. https://doi.org/10.1109/JSTQE.2018.2793945

Sancho J, Bourderionnet J, Lloret J et al (2012) Integrable microwave filter based on a photonic crystal delay line. Nat Commun.https://doi.org/10.1038/ncomms2092.

Sato H et al (2017) Low driving voltage Mach-Zehnder interference modulator constructed from an electro-optic polymer on ultra-thin silicon with a broadband operation. Opt Express. https://doi.org/10.1364/OE.25.000768

Schulz SA et al (2010) Dispersion engineered slow light in photonic crystals: a comparison. J Opt IOP 1:1

Sepehrian H, Lin J, Rusch LA, Shi W (2019) Silicon Photonic IQ modulators for 400 Gb/s and beyond. J Lightwave Technol. https://doi.org/10.1109/JLT.2019.2910491

Sinatkas G et al. (2021) Electro-optic modulation in integrated photonics. APL Photonics. https://doi.org/10.1063/5.0048712

Soares FM (2006) Photonic integrated true-time-delay beamformers in InP technology. Dissertation, Technische Universiteit Eindhoven. https://doi.org/10.6100/IR612707

Taddei C (2018) Advanced photonic signal processing and hybrid integrated microwave photonic systems. Dissertation, University of Twente. https://doi.org/10.3990/1.9789463234313

Taddei C *et al*. (2014) Fully reconfigurable coupled ring resonator-based bandpass filter for microwave signal processing. MWP) and APMP International Topical Meeting. https://doi.org/10.1109/MWP.2014.6994485.

Toroghi S, Fisher C, Khan S, Fathpour S (2016) Performance comparison of grating-assisted integrated photonic delay lines. J Lightwave Technol. https://doi.org/10.1109/JLT.2016.2619182

Urick VJ Jr, Mckinney JD, Williams KJ (2015) Fundamentals of microwave photonics. Wiley

Wang J, Shen H, Fan L et al (2015) Reconfigurable radio-frequency arbitrary waveforms synthesized in a silicon photonic chip. Nat Commun. https://doi.org/10.1038/ncomms6957

Wang J, Ashrafi R, Adams R et al (2016) Subwavelength grating enabled on-chip ultra-compact optical true time delay line. Sci Rep. https://doi.org/10.1038/srep30235

Weigel PO et al (2018) Bonded thin film lithium niobate modulator on a silicon photonics platform exceeding 100 GHz 3-dB electrical modulation bandwidth. Opt Express 1:1. https://doi.org/10.1364/OE.26.023728

Wu X et al (2020) Low-chirp push-pull dual-ring modulator with 144 Gb/s PAM-4 data transmission. Opt Express. https://doi.org/10.1364/OE.399800

Xiang C et al (2018) Low-Loss Continuously Tunable Optical True Time Delay Based on Si3N4 Ring Resonators. IEEE J Sel Top Quantum Electron. https://doi.org/10.1109/JSTQE.2017.2785962

Xu X et al (2017) High performance RF filters via bandwidth scaling with Kerr micro-combs. APL Photon 1:1. https://doi.org/10.1063/1.5080246

Xu X et al (2019) Advanced adaptive photonic RF filters with 80 taps based on an integrated optical micro-comb source. J Lightwave Technol. https://doi.org/10.1109/JLT.2019.2892158

Yang H, Yun B (2020). J Phys: Conf Ser. https://doi.org/10.1088/1742-6596/1634/1/012173

Yegnanarayanan S, Trinh PD, Jalali B (1996) Recirculating photonic filter: a wavelength-selective time delay for phased-array antennas and wavelength code-division multiple access. Opt Lett. https://doi.org/10.1364/OL.21.000740

Yeniay A, Gao R (2010) True time delay photonic circuit based on perfluorpolymer waveguides. IEEE Photonics Technol Lett. https://doi.org/10.1109/LPT.2010.2069558

Zhang D, Feng X, Li X, Cui K, Liu F, Huang Y (2013) Tunable and reconfigurable bandstop microwave photonic filter based on integrated microrings and Mach-Zehnder interferometer. J Lightwave Technol. https://doi.org/10.1109/JLT.2013.2287091

Zheng P et al (2019) Performances of microwave photonic notch filter based on microring resonator with dual-drive modulator. IEEE Photon J. https://doi.org/10.1109/JPHOT.2018.2885783

Zhou Y et.al (2016) Modeling and optimization of a single-drive push–pull silicon Mach–Zehnder modulator. Photon Res https://doi.org/10.1364/PRJ.4.000153.

Zhou X, Yu J (2009) Multi-Level, Multi-Dimensional Coding for High-Speed and High-Spectral-Efficiency Optical Transmission. J Lightwave Technol. https://doi.org/10.1109/JLT.2009.2022765

Zhu Z et al (2019) Positive link gain microwave photonic bandpass filter using Si_3N_4-ring-enabled sideband filtering and carrier suppression,". Opt Express. https://doi.org/10.1364/OE.27.031727

Zhu C et al (2020) Silicon integrated microwave photonic beamformer. Optica. https://doi.org/10.1364/OPTICA.391521

Zhuang L (2010) Ring resonator-based broadband photonic beam former for phased array antennas. Dissertation, University of Twente. https://doi.org/10.3990/1.9789036530781

Zhuang L et al (2010) Novel ring resonator-based integrated photonic beamformer for broadband phased array receive antennas—part ii: experimental prototype. J Lightwave Technol. https://doi.org/10.1109/JLT.2009.2032137

Zhuang L et al (2015) Programmable photonic signal processor chip for radiofrequency applications. Optica. https://doi.org/10.1364/OPTICA.2.000854